Università degli Studi di Napoli Federico II

Scuola Politecnica e delle Scienze di Base
Collegio di Scienze

Dipartimento di Fisica "Ettore Pancini"

Corso di Laurea Magistrale in Fisica

TESI DI LAUREA SPERIMENTALE IN FISICA MEDICA

Rotational radiotherapy of breast cancer with orthovoltage x-ray beams

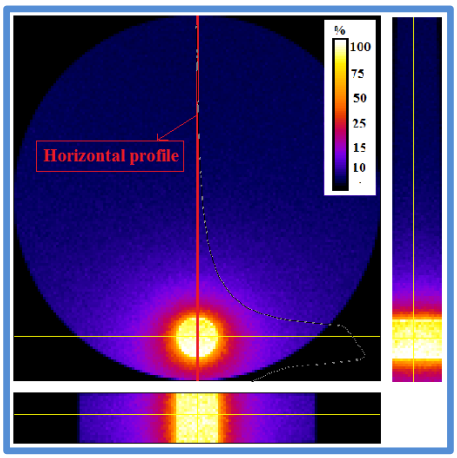

Relatori

Prof. Paolo Russo
Prof. Giovanni Mettivier
Dott. Antonio Sarno

Candidata

dott.ssa Francesca Buonanno
matr.N94000380

Anno Accademico 2016/2017

Sii grato per le sfide,
stanno creando la tua forza.

Summary

Introduction

Breast cancer is one of the most common malignancy in woman. Radiotherapy (RT) treatment was considered the gold standard of care for breast cancer after tumor mass surgery. The commonly therapy required 6 MV photons produced by a medical linear accelerator equipment. Megavoltage photons are beneficial given their characteristic depth-dose build up region whereby the dose to the breast skin is reduced to a fraction of the maximum dose deposit. Skin sparing is essential to avoid tissue complication after therapy.

In 2012 J. Boone and his team at University of California Davis proposed a novel technique of radiotherapy treatment dedicated to the breast cancer. They proposed to deliver RT on a platform developed for cone beam breast computed tomography (bCT) if equipped with an orthovoltage x-ray tube. Boone demonstrated the principle of rotational summation of the absorbed dose, so that is possible achieving an equivalent skin sparing using a collimated kilovoltage (kV) beam. This innovative technique was called kilovoltage external beam radiotherapy (kV-EBRT).

In this geometry the patient in prone position is laying with the breast pending from a hole in patient bed. The pendant breast was irradiated by the x-ray beam in a fully circular orbit, permitting to realize the summation of the dose in correspondence of the rotation axis. The effect is a dose distribution peacked at the centre of rotation.

Kilovoltage radiotherapy was commonly employed in clinical for treating skin cancer, as melanoma, since kV photons allow the maximum dose deposit at the surface. Treatment of deep-seated lesions with kilovoltage radiotherapy is under investigations by few research groups, for the simplified and more economical setup, respect to LINACs.

The aim of this work was to investigate, in an independent way, the feasibility of kV-EBRT technique for small tumor in breast cancer treatment by developing a dedicated Monte Carlo code. Partial breast irradiation was studied in terms of lesion-to-center dose ratio, which can explain a focused dose deposit on the tumour and, at the same time, skin sparing, as prescripted by the basic goal of radiotherapy treatment. Experimental measurements were performed in order to obtain an experimental validation of the code.

The thesis is divided in three chapters. In the first chapter we provided an overview of conventional breast radiotherapy treatment and illustrate, in detail, the idea of J. Boone and his

new kV-EBRT technique. A paragraph was dedicated to the kV arc therapy for treatment of deep seated tumor. In the second chapter we presented both the MC code developed via Geant4 toolkit to simulate the kV-EBRT and the simulations obtained for different irradiation geometry and beam energies. The MC code was experimentally validated, and in the third chapter we describe the experimental set up and the methods to achieve measurement with the kV- EBRT method. Finally, MC simulations were compared with measurements.

Chapter 1

Radiation therapy for breast cancer

Breast cancer is the most common cancer in women worldwide, and the second most common cancer overall. This represents about 12% of all new cancer cases and 25% of all cancers in women. It is the fifth most common cause of death from cancer in women [1]. The focus of this chapter is to provide essentials for breast cancer treatment. Firstly, are define basics of breast anatomy and treatment strategies for the cancer of the breast; then, is discussed conventional radiotherapy and the proposal of a new radiotherapic technique, the kV-EBRT (Kilovoltage Rotational External Beam Radiation Therapy), which is the object of this work.

1.1 Basics of anatomy of the breast

The mammary gland is composed of glandular tissue, subcutaneous fat, and dense and fibrous stroma containing an intricate network of lymphatics, nerves, and blood vessels. The breast is mainly situated on the pectoralis muscle and extends craniocaudally between the second and sixth anterior ribs and mediolaterally from the sternum to the axillary midline with a portion of the breast reaching into low axilla referred to as the "tail of Spance". Glandular tissue is made up of between 4-18 milk ducts emanating, not always radially, from the nipple-areola complex. The ducts branch terminates in ductal-lobular complexes (see Figure 1.1).

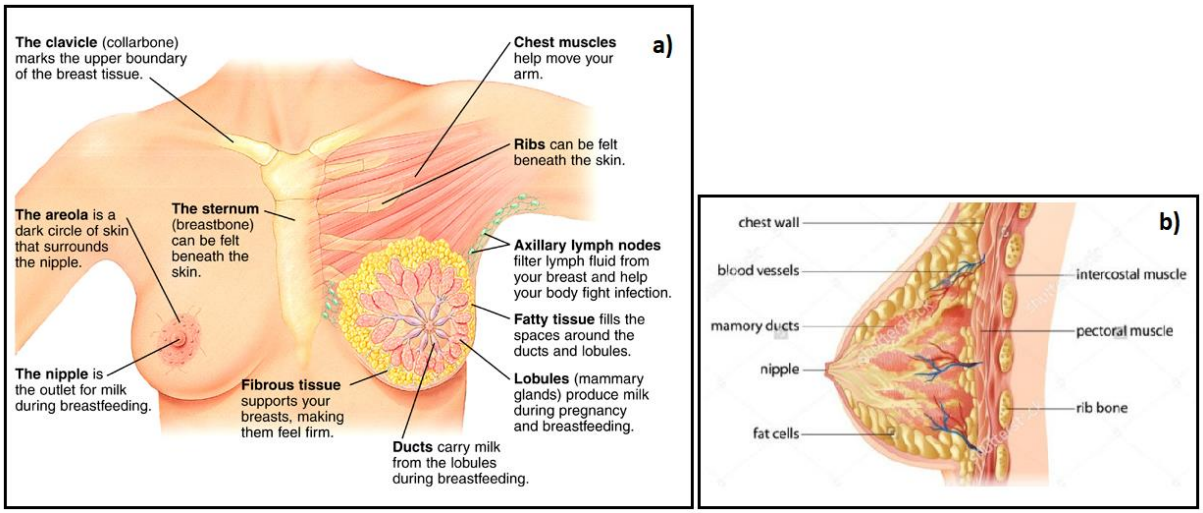

Figure 1.1. Image show breast anatomy. a) Frontal view. b) Side view. (https://uintageneralsurgery.com)

The lobules consist in specialized cells, which secrete milk that travel down the ducts to the nipple during lactation. Most breast cancer originate from the interface of the ductal-lobular complex.

One of the pathways cancer cells can use to travel to other parts of the body is lymphatic system. Lymph nodes and blood vessels can carry lymph through the body. In breast cancer the "sentinel node" is the first lymph node that a tumour drains into, so it's the first place that cancer is likely to spread.

A sentinel node biopsy is weightily to have information about the type of cancer: if there are cancer cells in the sentinel node, this means the cancer has likely spread outside the breast, and more lymph nodes will need to be taken out. But if no cancer cells are found in the sentinel node, this means the cancer has probably not spread and the other lymph nodes can stay (Figure 1.2.).

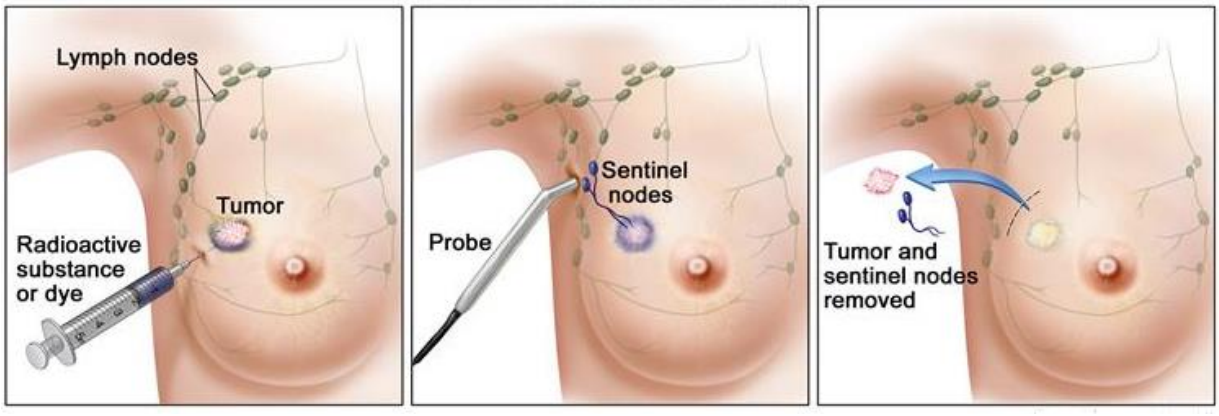

Figure 1.2. Sentinel lymph node biopsy of the breast. A radioactive substance and/or blue dye is injected near the tumor (first panel). The injected material is detected visually and/or with a probe that detects radioactivity (middle panel). The sentinel nodes (the first lymph nodes to take up the material) are removed and checked for cancer cells (last panel). (www.cancer.gov).

1.2 Overview on radiation therapy for breast cancer

The last decade has seen the development of new therapies and treatment strategies in terms of changes in our understanding of the biology of the disease, and on the other hand in terms of advances in radiation therapy techniques for breast cancer.

Radiotherapy (RT) in the management of breast cancer is typically given in the post-operative setting: surgery may address the primary cancer with either a lumpectomy (partial mastectomy) or a mastectomy. Breast conserving therapy for women with breast cancer consists of local

excision of the tumour (achieving clear margins) followed by radiation therapy. Post-operative RT sterilize tumour cells that may remain after surgery to decrease the risk of local tumour recurrence, reduce risk of ipsilateral breast tumour relapses (IBTR) about 75% compared to only surgery, have an impact to global survival of the patient, therefore RT is a basic technique for the treatment of this disease [2].

Whole breast irradiation (WBI) is the gold standard after conservative surgery or after total mastectomy. For early-stage disease and for minimal risk of relapse tumour is possible delivering radiation to a limited volume of the breast around the tumour bed (partial breast irradiation, PBI) sometimes with a shortened treatment duration (accelerated partial breast irradiation, APBI).

Both WBI and PBI treatments are delivered to the patient in several different sessions, for allow normal tissues to recover between fractions to a greater degree than tumour cells. Standard treatment contemplates 50.0-50.4 Gy up to a maximum of 60 Gy and fractionation typically refers to daily doses of 180 to 200 cGy in 5 sessions for week (for a total duration of treatment of 4-8 weeks), for balancing tumour killing and normal tissue sparing. The goal of PBI is primarily the reduction of duration of the RT. Indeed, in PBI patients receive an hypofractionation with daily doses of greater than 250 cGy. This have an impact on patient's waiting lists and on the discomfort of the patients, aspects of no secondary importance. Moreover, in PBI the irradiated volume is less than WBI, sparing organs at risk (skin, heart, lung). Radiotherapy is delivering with various planning and treatments methods, which are summarized in Appendix A.

The most common technique are the followers:

- Teletherapy or external beam radiotherapy (EBRT), refers to the delivery of radiation from a source external to the patient. Photons, electrons or protons can be used for EBRT; beams of these particle are generated using linear accelerators (photons, electrons) or cyclotrons/synchrotrons (heavy particles) and then directed to the target. As the particles interact with matter, they deposit energy in the target medium.
- Brachytherapy refers to delivery of radiation from sources placed inside the patient. With this technique high dose can be delivered to the tumour with nearby organs receiving much lower dose.

- Intra-operative radiotherapy (IORT) allows delivering boost of radiation dose during the surgery, after the excision of the tumour, directly on the area that contained the neoplasia. For this purpose, can be used photons of low energy or electrons produced by a dedicated mobile compact accelerator (LIAC, Light Intraoperative Accelerator).

All these techniques are valid only if properly selected. It's fundamental considering the position of the neoplasia, mammary volume, ratio of tumour volume versus glandular tissue, as well as the availability of the single centre of radiotherapy.

1.3 Conventional EBRT: planning and delivering

Traditional EBRT is based upon application of x-ray beam produced by medical linear accelerators (LINAC) in order to irradiate the breast. Modern linear accelerator operate in the MV range, indeed can generate MeV photons, typically with energies of 4-20 MV.

In figure 1.3. we can see a LINAC and treatment table. If desired, the gantry can rotate 360 degrees to provide treatment from any angle. These machines have an isocentre set up for precise calculation when determining the relationship between patient position and treatment machine position. Beams are shaped to match the shape of the target volume trough using multiple collimators (multileaf collimators) that can move during the RT session to better shape dose. Shaping the beam is an important way of minimizing the absorbed dose in healthy tissue and critical structures [3].

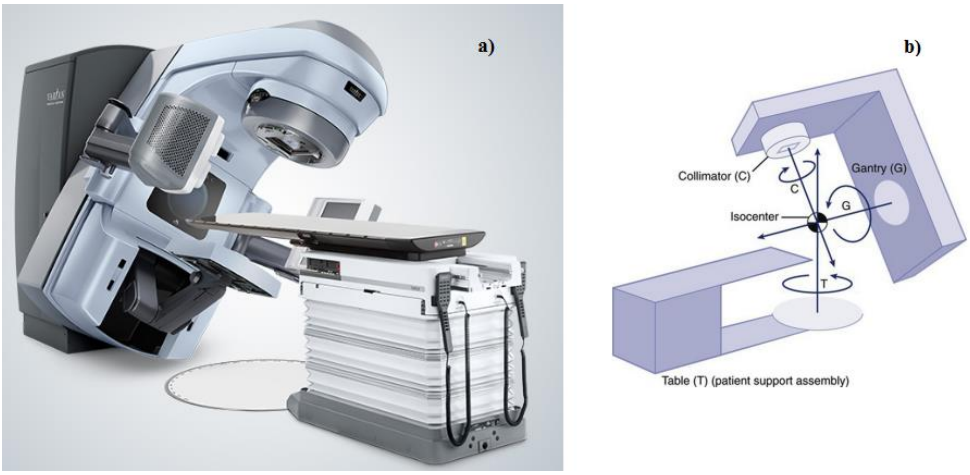

Figure 1.3. a) Image show an example of LINAC: Clinac® iX System (https://www.varian.com/en-au/oncology/products/treatment-delivery). b) Isocentre of a gantry-based radiotherapy machine. The gantry, collimator and table all rotate around a single point, called isocentre [4].

Before treatment is necessary the identification of target and normal tissue volume using computed tomography (CT) imaging or magnetic resonance imaging (MRI). Once target volumes and normal tissue are identified the radiation oncologist prepares a prescription document that identified the desired dose and fractionation schedule. Medical Physicists use treatment planning software (TPS) to design a treatment plan that meets the prescription document.

The optimal plan finds a balance between target coverage and normal tissue sparing. There are some organs that are more sensitive to radiation therapy like heart, lungs, spinal cord, called organs at risk (OAR).

Many studies [5,6] affirm that RT treatment for breast cancer involves in unwonted irradiation of the heart and this may result in an increased risk of heart disease. Is observed in women with left-sided breast cancer higher cardiac mortality compared with woman with right-sided cancers. This is favourite by the fact that RT is delivered with the patient in supine position, like we see in figure 1.4.

Figure 1.4 Conventional external beam radiotherapy. Figure shows a patient in supine position on the treatment bed of a LINAC gantry. (http//www.hindawi.com)

In breast cancer treatment other organ at risk is lung. So, it's very important try to minimize dose to the heart and lung balancing benefits of the treatment and limit the irradiation of these OAR. In figure 1.5 we can see a CT slice in coronal view used to identify target and normal tissue during the planning of RT. In figure 1.6 is show an example of TPS for WBI: the treatment

contemplates two opposite tangential fields to cover the breast (and the chest wall or low axilla nodal levels if indicated).

Management strategies that reduce dose to OAR are respiratory gating (the machine irradiate only when sensors on patient detect that the lungs are included above a certain threshold), prone positioning, partial breast irradiation. Overall, cardiac sparing is more difficult for patient with left-sited tumours.

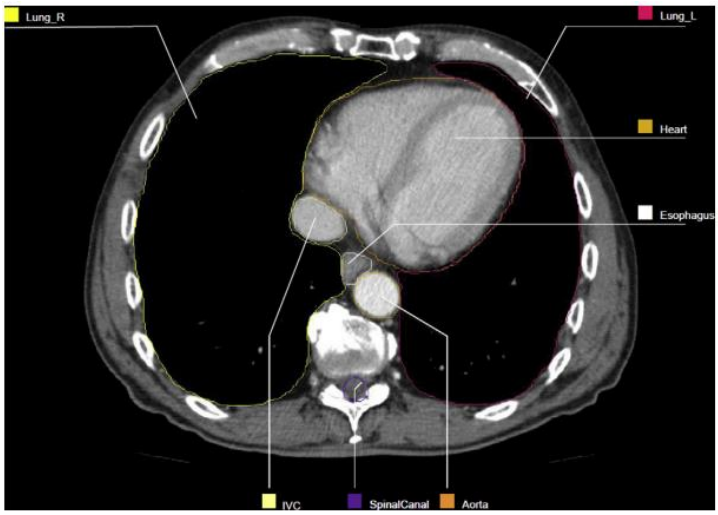

Figure 1.5 CT slice in coronal view. We can see normal tissue contours to allow the planning system to calculate dose to the specified organs. We can observe contouring with different colours of lungs, heart, oesophagus, IVC (inferior vena cava), spinal canal, aorta [4].

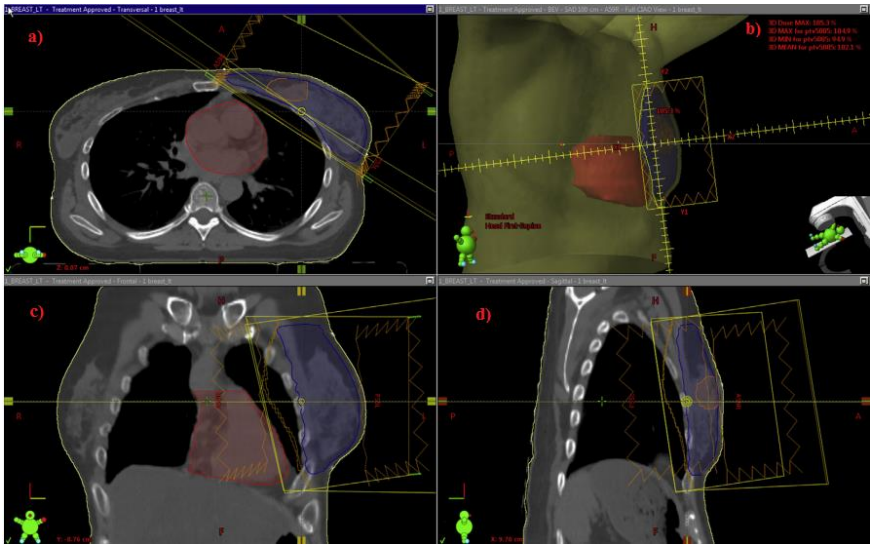

Figure 1.6 TPS for whole breast therapy. a) Axial view. In blue we can see the target, in red the heart. b) Beams' projection of the medial tangent field. c) Coronal view. d) Sagittal view [4].

1.3.1 Conventional EBRT: Megavoltage photon beams

The purpose of this paragraph is to explain physical properties governing radiation therapy to understand the characteristic of radiation to give both therapeutic and toxic effect on patients.

LINACs used for treatment delivery work typically at 6 MV, producing some x-ray spectrum with photons presenting all energy from 0 to a maximum value of 6 MeV, which is equal to the kinetic energy of electrons striking to the target. Dose deposition from a megavoltage photon beam exhibit the "skin sparing" characteristic due to dose build up region about at 1.5 cm from the skin of the patient.

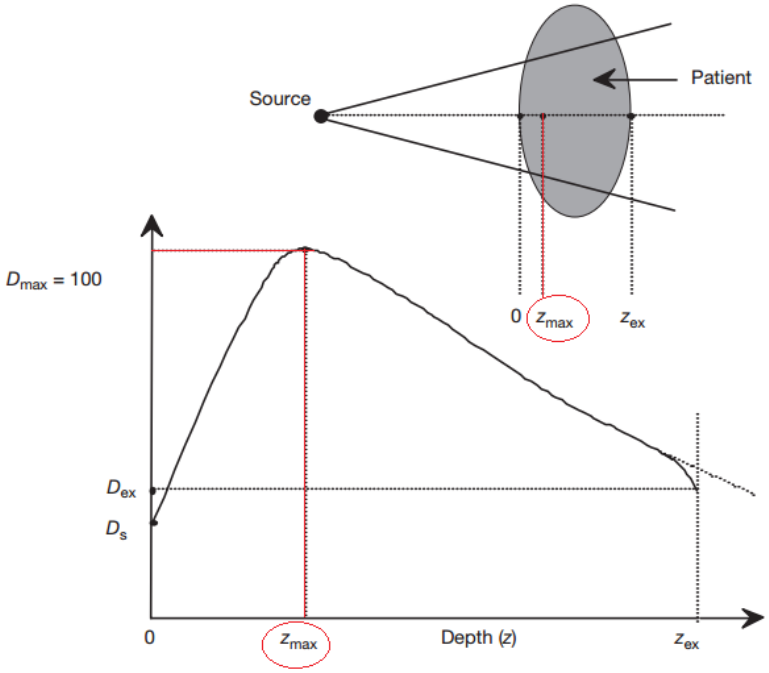

Figure 1.7 Figure show a typical dose distribution on the central axis of a megavoltage beam. D_s is a superficial dose, at z_{max} depth dose reach a maximum value D_{max}, D_{ex} is the dose delivered to the patient at the beam exit point z_{ex}: we can observe a small curve downwords due to missing scatter contribution at the exit point from point beyond the exit dose point [7].

Figure 1.7 shows a typical dose distribution on the central axis of a MV x-ray beam. Radiation enter in the patient on the skin surface, where delivers a certain surface dose D_s, then the dose first rise rapidly, reaches a maximum value D_{max} at depth z_{max}, finally decreases exponentially until it reaches a value D_{ex} at the patient's exit point. The build-up effect can be explained in the fallowing way: for a megavoltage x-ray beam interact with the medium (photoelectric effect, Compton effect, pair production) are released a long range energetic

secondary electron, that deposit their energy so far from their point of origin. Next, energy fluence decreases exponentially following the Lambert Beer's law:

$$\frac{\psi}{\psi_0} = e^{-\mu x}$$

Where ψ is the energy fluence (MeV/cm^2) at depth x in matter, $\psi_0$is the energy fluence of the primary beam, and μ is linear attenuation coefficient, measured in cm^{-1}.

Surface dose and depth of dose maximum depends mainly on beam energy (see figure 1.8). Skin receive amounts 15% of the maximum dose for a 6 MV x-ray beam and 10% for an18 MV x-ray beam [7].

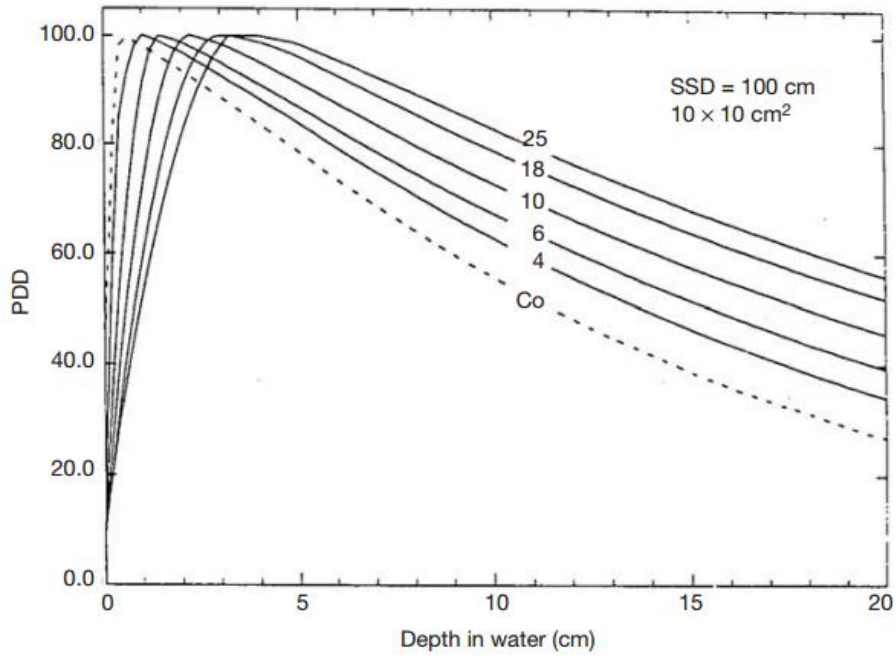

Figure 1.8 Percentage depth dose curves for megavoltage x-ray beams with energies from Co γ rays (to 25 MV at an SSD (source to surface distance) of 100 cm for a 10x10 cm^2 field. Build up region increase with increasing of photons energy. The maximum dose at 6 MV is at 1.5 cm depth, at 25 MV maximum dose arrive at 5 cm depth [7].

1.3.2 EBRT: Kilovoltage photon beams

Before the invention of LINACs kilovoltage x-ray beams were the only modality of RT and were used to treat even deep-seated tumour. Actually, orthovoltage (150-300 kV) and superficial (50-150 kV) beams are used to treat skin cancer, such as melanoma, squamous cell carcinoma (SCC) and basal cell carcinoma (BCC) as well as non-malignant skin conditions such as keloids,

exploiting their characteristic dose deposition (see figure 1.9). Relatively high absorption of these low energy x-rays in bone also means that orthovoltage treatment is well suited to the palliative treatment of painful bony metastases in shallow regions such as the ribs and sternum. It is estimated that the 73% UK radiotherapy centres have at least one clinical kV therapy unit, with a total of 58 unit that treat approximately 6000 patients each year [8].

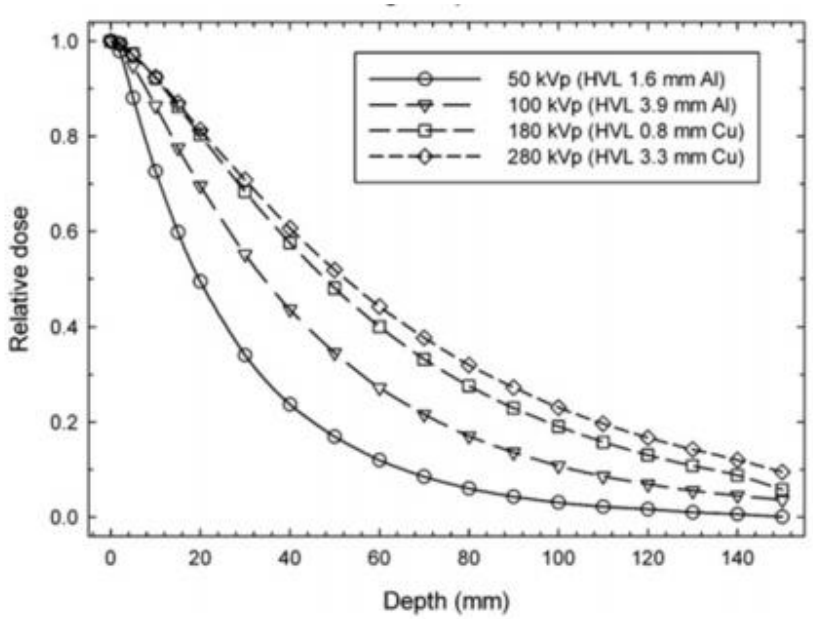

Figure 1.9 Percentage depth dose curves for kilovoltage beams with energies from 50 to 280 kVp. The dose at surface in nearly to 100% for beam energies in the kilovoltage range. The relative dose at 280 kVp at 2, 10 and 20 mm depth is approximately 99%, 93%, 82% respectively and drops to 50% at 5 cm depth [9].

Orthovoltage and kilovoltage beams do not exhibit the skin sparing effect, since their dose maximum occurs on the skin surface, then the dose delivered decreases (falls off) rapidly as depth of the medium increases. Megavoltage x-ray are more penetrating, which means that these beams are more indicated for treating deep-seated tumour. Figure 1.10 show a clinical device operating for superficial and orthovoltage treatment in a range from 15 kVp to 300kVp. Typical depths of dose maximum z_{max} for various photon beam energy and field size of 5x5 cm^2 are shown in Table 1.1.

	Superficial	Orthovoltage	Co-60	4 MV	6 MV	10 MV	18 MV	25 MV
z_{max} (cm)	0	0	0.5	1	1.5	2.5	3.5	5

Table 1.1 Table show value of z_{max} for x-ray beams of different energies. The skin sparing effect is present only for MV beams. For superficial and orthovoltage the maximum dose deposition is at surface of the medium [7].

Figure 1.10 T300 orthovoltage machine available for clinical application. The high tension (from 15 to 300 kVp) and the tube current output of the tube can be combined with different clinical filters to a great number of HVL combinations. Type of x-ray tube is MXR 321 (http://www.tur-x-ray.com/therapy/).

1.4 Kilovoltage rotational external beam radiotherapy (kV-EBRT) for breast cancer

This paragraph has the aim to present the topic of this thesis work, the kV-EBRT technique, firstly proposed in 2012 by Professor John Boone of University of California and his research group at Davis Medical Centre, Sacramento, California.

As seen in previous paragraphs, the basic goal of radiotherapy treatment is the irradiation of a target volume while minimizing the amount of radiation absorbed in healthy tissue. A conventional EBRT for breast cancer provides for use of 6 MV photons to ensure skin sparing. Boone's work demonstrate that an equivalent skin sparing can be achieved from rotational summation of a collimated kV beam delivered by a breast computed tomography (bCT) platform, an experimental tomographic cone beam x-ray-based imaging that generate 3D images of the pendant breast. [9]. The study demonstrates, via Monte Carlo simulation, the feasibility of a dedicated bCT platform to deliver rotational kV-EBRT for PBI, WBI and dose painting applications.

1.4.1 Basic aspects of bCT

In 2001 Professor Boone and his team at University of California at Davis, UC Davis, proposed a new technique for bCT with a dedicated scanner, a technology capable of producing CT images of the whole uncompressed breast, in opposition to traditional screening mammography, where the breast is under a plat of compression, necessary to obtain contrast in the images [10].

The geometrical scheme proposed by Boone is the following: an x-ray beam from a tungsten anode, collimated to a half-cone geometry irradiates the uncompressed pendant breast of prone woman while both tube and detector rotating 360 degrees around a vertical axis, obtaining several hundred projections (figure 1.11). A depression in the patient's bed allows to put the chest wall at the height of the central axis of the x-ray tube. The 3D reconstruction from projections is obtained using typical algorithm used for conventional fan-beam CT [11]. In 2005 UC Davis team developed the first prototype of bCT operating at 80 KVp, which was called "Albion". In Albion the geometry is fixed (source to image distance was 1 m) and acquisition occur in continuous mode in a scan time up of 16.6 s during which the patient is in a breath-hold condition to produce small motions artefacts. Three others prototype scanners were proposed by Boone's team increasingly sophisticated.

From 2001, several research groups in the USA and in the European Union were inspired to develop bCT system dedicated to breast imaging.

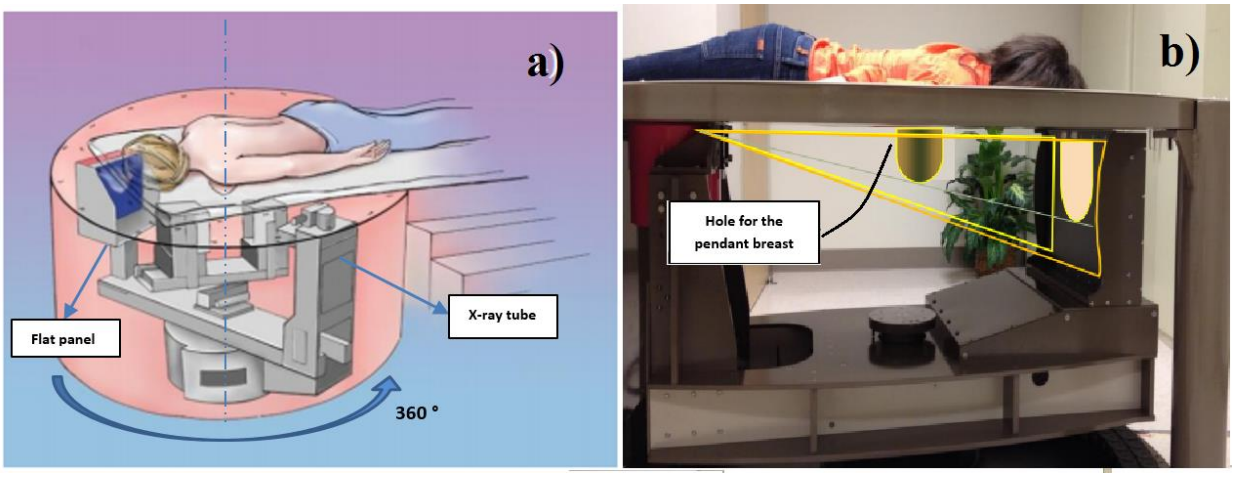

Figure 1.11 a) The figure shows prone position of patient under bCT. The breast of the patient is pendant and under the gantry both x-ray tube and flat panel rotate 360 degrees around the breast. b) bCT scanner prototype developed at Davis Medical Centre (US Davis), called Bodega. The system has a hole in which the breast can be inserted. The x-ray tube is mounted over rotating platform.

Since 2007 the working group of Medical Physics coordinating by Professor Paolo Russo of the University of Naples "Federico II" has developed laboratory prototypes of cone beam micro CT dedicated to the breast. So, because of the availability of a bCT scanner in own Medical Physic laboratory the idea to study kV-EBRT was taken into great consideration since 2012, after the publication of Boone's work about the feasibility to kV-EBRT with bCT system.

1.4.2 kV-EBRT technique by Prionas et al.

The idea of Professor Boone is using the geometry of bCT scanner to perform rotational kV external beam RT if it is equipped with an orthovoltage (100-500 kV range) x-ray tube. We have seen that in opposition to breast RT delivered using 6 MV photons, that have the plus of be "skin sparing", orthovoltage photons deposit the maximum dose on skin surface, because there is not any build up region.

On the other hand, x-ray produced by an orthovoltage tube are less energetic and so deposit less dose in the patient. The dose delivered to the skin is minimized from rotation of the gantry because in each position during the rotation the skin receive only a small quantity of dose. The result is that with this technique is possible to achieve a good skin sparing, also is insured the dose to tumour for the principle of summation of the dose during the rotation (the axis of rotation of the gantry pass through the tumour). In figure 1.12 we can see the configuration to perform kV-EBRT. Moreover, the system is born to perform diagnostic breast imaging, so we can realize both RT and imaging during the treatment: image-guided radiotherapy (IGRT). The IGRT technique reduce patient repositioning error and recover treatment accuracy. It allows to obtain an adaptive RT, in fact the treatment plan can change based on observed anatomic changes of the patient, weight loss, internal motion, for example. Adaptive RT can be performed immediately prior to a treatment and in real time during the treatment.

Another goal of kV-EBRT is the prone position of the patient during the treatment. Many studies compared WBI in prone versus supine position. These studies showed that prone position leads to reduce heart and lung doses in breast cancer treatment, and so reduce the risk of ischemic heart disease and radiation-induced lung cancer [5,6].

For patients with positive lymph nodes conventional RT in supine position inhibit delivering sufficient dose to axillary lymph node regions, but on the other hand prone position is not desirable for regional nodal irradiation: the support material obstruct the beams access to lymph nodes, which can create a build-up effect with more skin dose and not sufficient dose to lesion

in the axilla [12]. This aspect is object of many studies and for the moment the standard in RT remain supine position, especially when lymph node irradiation is required.

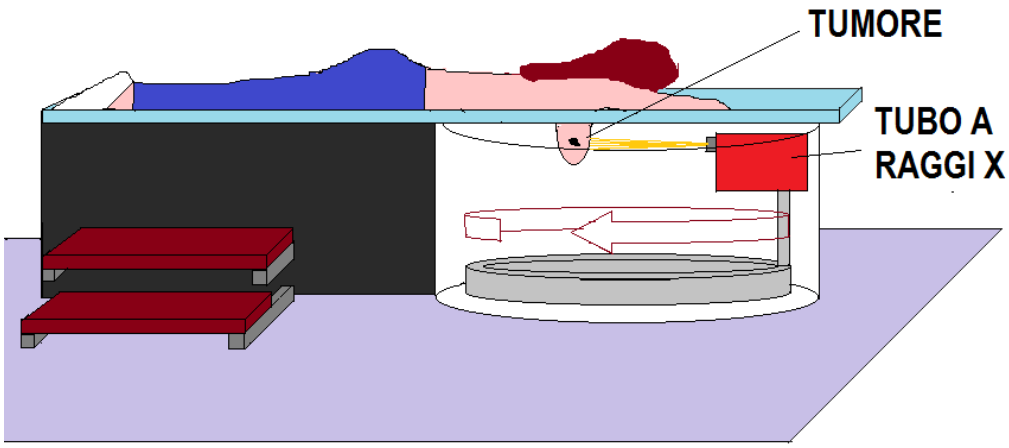

Figure 1.12 Figure show the bCT set up for deliver kV-EBRT. An x-ray tube rotating 360° around pendant breast of patient to perform both RT and acquisition of CT images (from: De Lucia P. A. Presented at National Congress of the Italian Society of Physics, Rome, Italy, 25/09/2015).

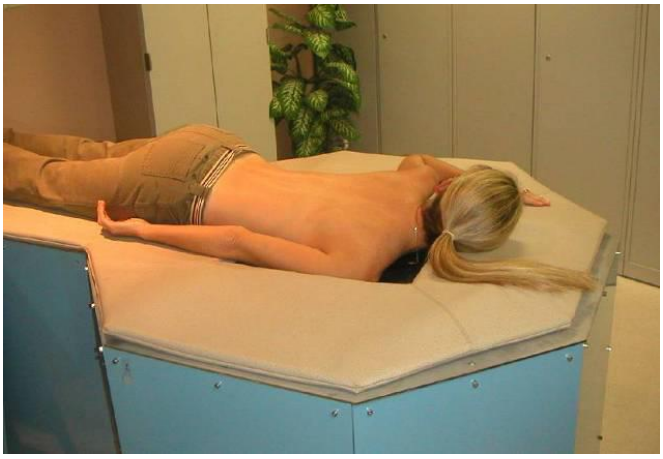

Figure 1.13 Woman in prone position on bCT scanner equipped for kV-EBRT. This image was made from research group of Medical Physics of US Davis to show the placement on their prototype of bCT platform (www.ucdavis.edu).

Summarizing, the advantage of kV-EBRT respect conventional RT are:

- breast CT platform is smaller and simpler than LINACs, can be placed easily on the ground floor of a radiotherapy centre to ease the access for the patient, as opposed to LINACs equipment which requires a bunker;
- this system is less expensive than conventional RT, using x-ray tubes;

- possibility to perform IGRT;
- prone position reduced heart and lung doses;
- improved patient comfort and dignity.
- provide a single system for both targeting and delivering therapy, with more accurate treatment delivering and shorter treatment times.

The result of this technique is a focus of dose deposited around the target, as piqued as it is collimated the x-ray beam in the horizontal direction, with a rapid dose fall off in the medium. The central axis of rotation mast be placed on tumour. This allows to treat small volumes (PBI), with the breast skin receiving only a small fraction of the dose. It's also possible to perform a WBI and dose painting using multiple rotations varying beam collimations widths.

The clinical feasibility of kV-EBRT was demonstrated by Boone et al. via Monte Carlo (MC) simulation and experimental measurements.

The simulations were performed with N-Particle Extended radiation transport code (MCNPX 2.6.0) and were based on the same geometry of the prototype bCT platform with a 51.1 cm source-to-isocentre-distance (SSD). A 14 cm diameter polyethylene disk or cylinder (0.9325 g/cm^3), which represent pendant breast of average diameter, was irradiated at isocentre, positioned at centre of the cylindrical phantom, with an x-ray spectrum of 320 kVp (half value layer of 4.4 mm Cu) generated with MCNPX.

Simulation of depth dose characteristic at 320 kVp has demonstrated that the same depth dose curve can be obtained with monoenergetic photons at 178 keV, like we see in Figure 1.14. So, for simplicity all the other simulations were performed at 178 keV.

Beam collimation was set to 0.1 cm or 2 cm in the z direction and varied from 1 to 14 cm in the x-y plane. Figure 1.15 shows the geometry used to perform simulations.

Two dimensional and three-dimensional dose profiles were generated using:

- voxelized (0.1 cm isotropic voxels) disk 0.1 cm tall, to simulate the primary photon interaction;
- voxelized (0.1 cm isotropic voxels or 0.5 cm isotropic voxels) cylinder 9 cm tall to simulate the primary and scattered photons.

The results of 2D distribution are plotted in in terms of percent of central dose (percentage of dose along the radial profile of the cylinder normalized for the value of dose at isocentre) as function of radial distance from the axis of the cylindrical phantom (Figure 1.15).

Simulations using a 14 cm beam (the beam irradiate all the virtual phantom) resulting in a 2D dose distribution with a cupped profile. The surface dose is about 160% of the maximum dose deposited in the medium and this is the dose that ideally would be absorbed from the skin.

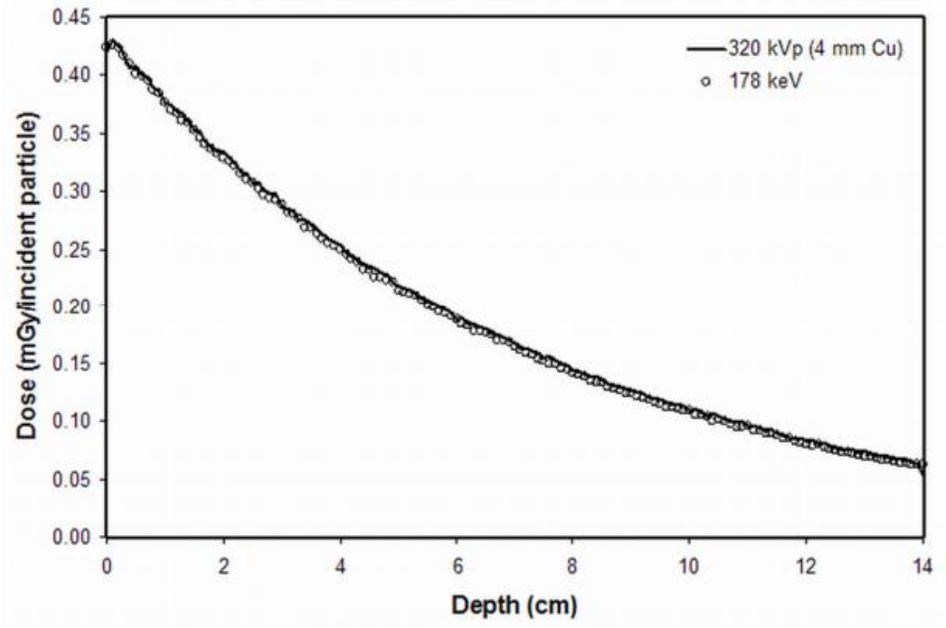

Figure 1.14 The graph show simulated depth dose curve for 178 keV monoenergetic photons matched with 320 kVp x-ray beam filtered with 4 mm Cu (HVL= 4.4 mm Cu). (supplementary material of Boon's Study [9], available at www.redjournal.org.).

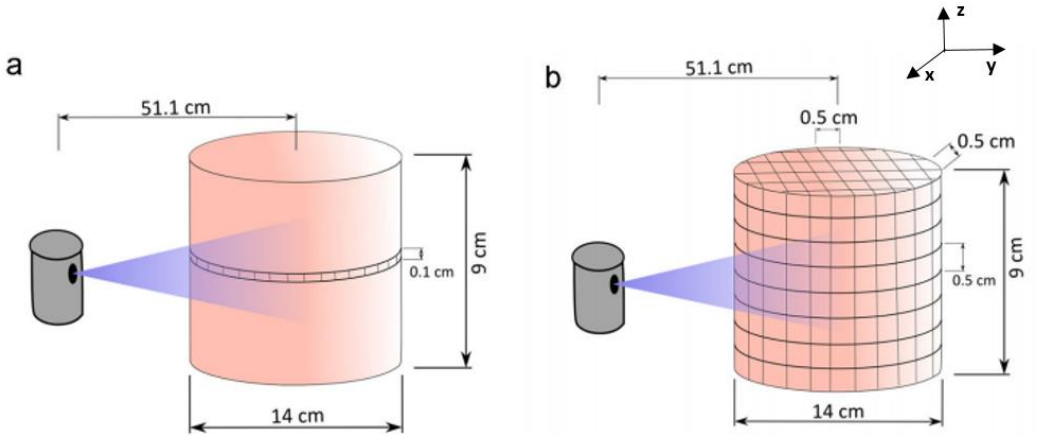

Figure 1.15 Geometry simulation used to generate a) 2D dose distribution. b) 3D dose distribution (supplementary material of Boon's Study [9], available at www.redjournal.org.).

While with 1 cm of x-y collimation the 2D dose distribution showed a pecked dose deposition, with the surface dose lower than 7% of the maximal dose. That means that, ideally, the tumour

receives the maximum dose deposition, achieving a good skin sparing. The width of the peak depends on beam collimation.

Rotational kV-EBRT was simulated also using CT coronal slices acquired on the bCT scanner, which contains a cancer lesion in the middle. The images were previously segmented to differentiate the tissue of the breast and then are sandwiched between polyethylene for a total height of 9 cm. The lesion was completely irradiated with a beam 2 cm x-y collimated and 0.1 cm z-collimated. Figure 1.17 show that the lesion was within the 90% of isodose line, and the skin receive approximately 10% of the maximum dose. The dose deposition in adipose and glandular tissue was similar.

Prionas et al (2012) demonstrated the feasibility of the kV-EBRT technique with good skin sparing for both PBI and WBI and for dose painting and proposes that bCT platform has the potential to deliver kV-EBRT with many benefits than conventional supine megavoltage breast RT, as we discuss in the previous paragraph. These results are only the first step before this innovative technique enter in the clinic; the way is so hard, but the premises are very good in terms of guarantee skin sparing focusing adequately dose on the tumour.

The clinical feasibility of kV-EBRT necessitate a bCT platform with a dynamic multileaf collimator, an x-ray tube capable of rapid tube current modulation and a slip-ring gantry for source rotation. A critical aspect of this technique is the necessity to have high-power tube capable of delivering sufficient dose rate.

Technical data for a similar orthovoltage source indicate that it is possible to obtain a dose rate of 1Gy/min at 50 cm source-to-surface distance. Compared with MV EBRT, where typical dose rate is about 500 cGy/min for a total beam on of 2 min, the treatment with kV-EBRT is expected to be longer for the same dose prescription. However, the total time of the procedure can be similar to conventional treatment (that can approach about 15 min), thanks to the simplicity of patient and source positioning on the bCT platform.

After this work many research groups have taken in great consideration this technique, and others feasibility studies were realised. In the following paragraph will be descript the works, published from 2016, of a Canadian research group coordinating by M. Bazalova-Carter, working at University of Victoria, Victoria, Canada.

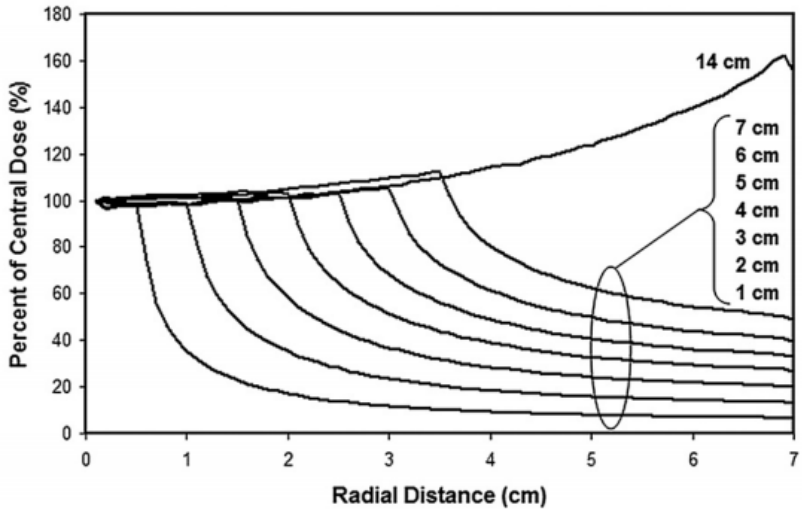

Figure 1.16 Dose profile for the beam of x-y collimation increased from 1 to 14 cm. As the width of the beam increase dose deposition shape like a half cup [9].

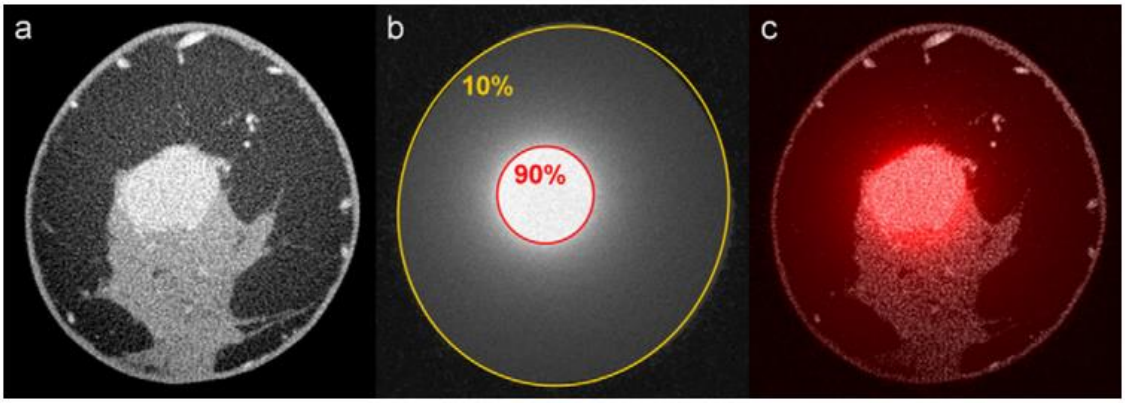

Figure 1.17 a) bCT coronal slice containing invasive mammary carcinoma used to simulate kV-EBRT with a beam 2 cm x-y collimated and 1 cm z-collimate. b) isodose distribution after the irradiation in grey scale: 90% of maximum dose was delivered to the lesion (in red) while only 10% to the skin (in yellow), c) fusion of image a) and b) in red scale [9].

1.4.3 Kilovoltage arc therapy (kVAT) technique by M. Bazalova-Carter

The kVAT technique proposed in 2016 by Bazalova-Carter et al. is based on the idea to treat deep-seated tumour using a novel kilovoltage x-ray source rotating along arcs and able to conform the dose to targets with high skin sparing.

The Canadian's group demonstrated via MC simulations that it's possible performing conformal treatments of deep-seated tumour whit kilovoltage x-ray with dose distributions comparable to MV beams, with estimated cost approximately 10% of the cost of a modern LINAC [14].

The kVAT source was modelling on an existing multi-focal-spot diagnostic kV x-ray source. The original source, used for diagnostic imaging, consisted of a 2D array of 100x100 x-ray beamlets generated by an electron beam scanned on a large tungsten anode and shaped by a collimator. The kVAT source was built via MC simulations performed with the EGSnrc/BEAMnrc (V4 2.4.0) code and was re-arranged in a linear array as well as the collimation system was optimized, to perform kVAT.

In figure 1.18 a) is show a scheme of the proposed source: an electron beam was simulated as monoenergetic pencil beam for each collimator hole, electrons travelled for 20 cm in vacuum before impacting with the anode producing x-ray spectrum for bremsstrahlung. Nine collimator holes of 3 mm diameter at the anode adjacent spread across 50 cm so that nine x-ray beams just cover the lesion.

This x-ray source was designed to treat a 4 cm diameter spherical target at 10 cm depth in a 40 cm diameter cylindrical phantom of soft tissue (ICRU-44 data), modelling to simulate the human torso and a 120° arc treatment was considered for a source to axis distance (SAD) of 45 cm. The isocentre match with the centre of the target (Figure 1.18 b). An illustration of the geometry of this treatment system, including gantry, source and couch is shown in Figure 1.19. Dose to phantom was calculated for firstly for the default set of parameters:

- 200 keV electron beam energy;
- 17 μm anode thickness;
- 0.4 mm al added filtration;
- 9 collimator holes of 3 mm diameter spread over 50 cm;
- 10 cm collimator thickness;
- 45 cm SAD;
- 120° treatment arc.

Dose distributions achieved setting default parameters are showed in Figure 1.19. For a single stationary 200 kV beamlet the target dose was less of 10% of the maximum dose (D_{max}) that was deposited in the skin; for all nine stationary beamlets the dose to the target increased to 30% of D_{max} thanks to contribute of the lateral beamlets. On the contrary if it was added the rotation along 120° arc the nine beamlets generate a dose distribution with a dose to the target of 70% of D_{max} while the skin dose decreased to 50% of D_{max}. If the same treatment was delivered lateral

beamlet weighting, the target dose increased to 80% of D_{max} and skin dose decreased further to 30%.

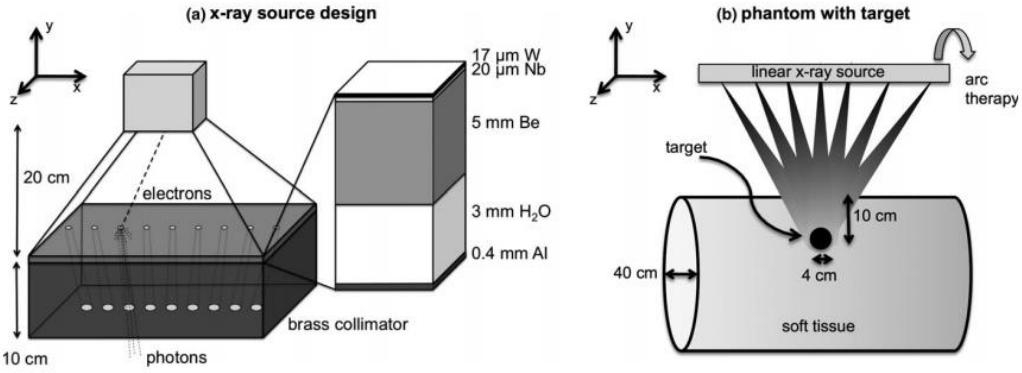

Figure 1.18 a) A scheme of the kVAT x-ray source. The idea is that pencil beams of monoenergetic electrons impact on a 17 µm tungsten anode, producing corresponding x-ray beams. Following: 20 µm niobium layer, 5 mm beryllium window, 3 mm thick water cooling layer and 0.4 mm thick aluminium filter. b) A scheme of the geometry simulated for kV-arc-therapy: the linear x-ray source irradiates a deep-seated target of 4 cm diameter at 10 cm depth in a 40 cm diameter cylinder [14].

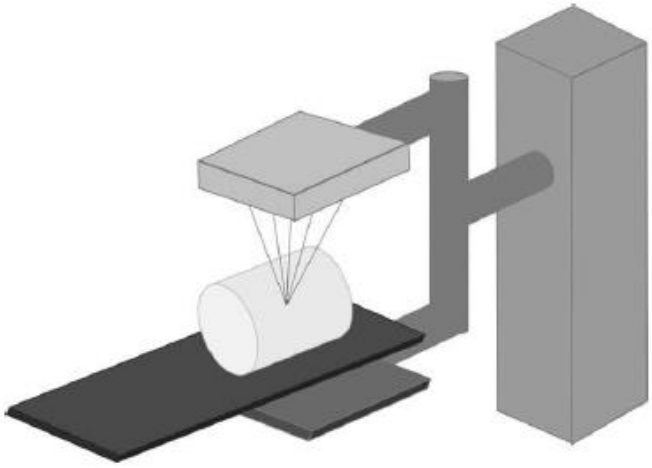

Figure 1.19 Illustration of a feasible kVAT system geometry. The figure show the gantry, arm, couch treatment source and kV image detector panel [15].

Source output depends closely from input parameters. Varying treatment parameters and their effect on the quality of dose distribution was evaluated. For this purpose, was developed a MATLAB code to automatize the generation of the input data for the source based on target size. Dose to target volume was evaluated in terms of D_{50} (the dose delivered to 50% of target volume) to compare to radiosurgical dosing prescriptions and dose sparing to healthy tissue in terms of target-to-skin ratio.

A set of optimized parameters was obtained follow-on the maximum target-to-skin ratio with a clinically acceptable D_{50} during 30 min of irradiation. The results of the parameter study are presented in Figure 1.20.

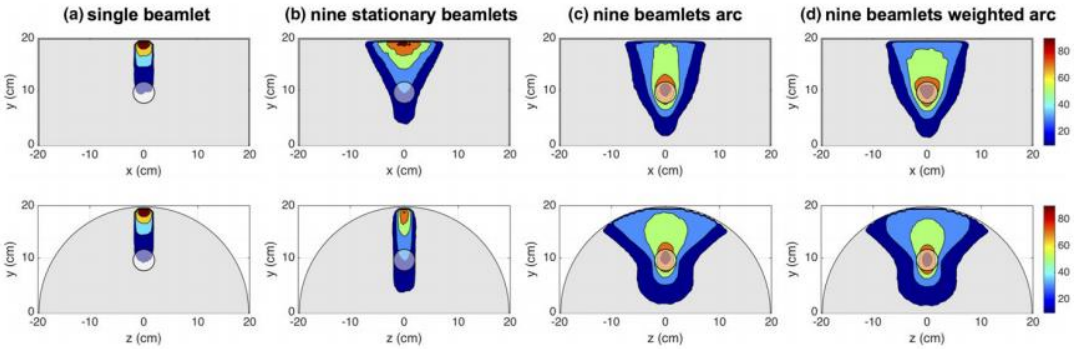

Figure 1.20 Sagittal (on the top) and axial (on the bottom) view of dose distribution for 200 kV x-ray beams; the maps are presented in false colours from blue (low percentage of D_{max}) to red (high percentage of D_{max}). a) single beamlets. b) nine stationary beamlets. c)120° arc therapy with nine beamlets. d) 120° arc therapy with nine beamlets with increased beam weighting for peripheral beamlets [14].

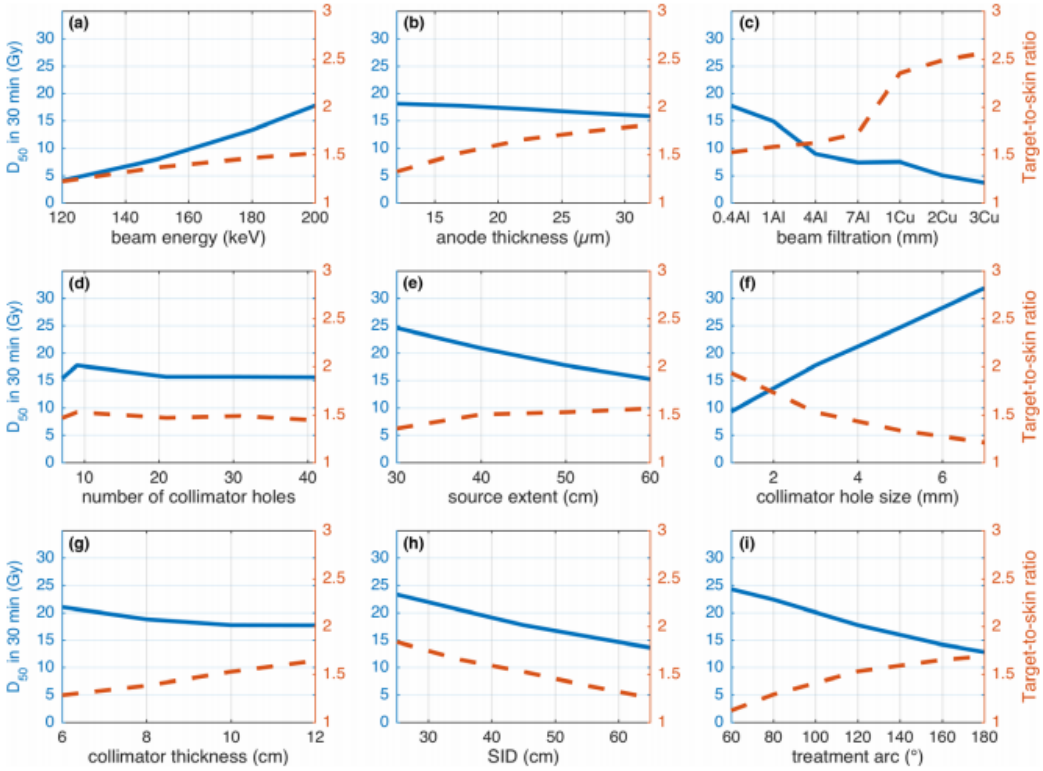

Figure 1.21 Figure show D_{50}(solid line) and target-to-skin ratio (dashed line) as function of; a) beam energy, b) anode thickness, c) beam filtration, d) number of collimation holes, e) source extent f) collimator hole size, g) collimator thickness, h) source-to-isocentre distance, i) treatment arc [14].

The optimized parameters are setting as the following:

- 200 kV electron beam energy;
- 32µm anode thickness;
- 0.4 mm Cu added filtration;
- 9 collimator holes of 5 mm diameter spread over 60 cm;
- 10 cm collimator thickness;
- 20 cm SAD;
- 120° treatment arc.

The optimized dose distribution was show in figure 1.21. All doses are shown in Gy normalized to dose delivered in 30 min. We can see that the skin dose was within 10%.

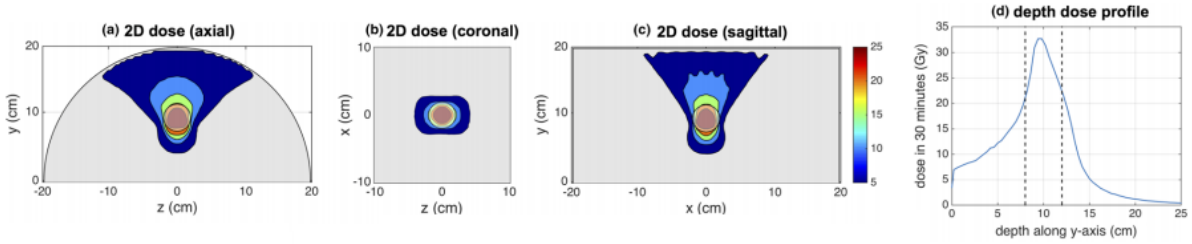

Figure 1.22 Optimized dose distribution in the a) axial b) coronal c) sagittal views for 200 kV beam filtrated with 0.4 mm Cu. These maps are presented in false colours from blue (low dose normalized to dose delivered in 30 min) to red (high dose normalized to dose delivered in 30 min). Figure d) shows dose profile along the y-axis [14].

The optimized kVAT generated a conformation plan whit a target-to skin-ratio of 5.1 and D_{50} in 30 min of 25.3 Gy. That dose would be, in prospective, an optimal dose prescription in radiosurgical ablative treatment.

MC kVAT dose distribution was also calculated for CT images of a patient's abdomen with a pararenal target located at 12 cm deep. The target was modelling whit an equivalent sphere diameter of 1.6 cm. The kVAT dose distribution was compared to a 15 MV VMAT (Volumetric Modulated Arc Therapy) dose distribution and results are presented in figure 1.22. As we can see in figure, the 200 kV and 15 MV VMAT dose distributions resulted in a comparable isodose lines. For both techniques the target was covered by the 99% of the isodose line and the maximum target dose was 108% for 200 kV kVAT and 105% for 15 MV VMAT of the prescription dose.

Bazalova et al, with this work, demonstrated the feasibility of the new kVAT technique with an optimal percentage of prescription dose, in terms of D_{50}, delivered to the deep-seated lesion with a skin sparing within 10%.

However, limitations due to acceptable skin dose restrict the size of treatable lesions with this technique. In 2017 D. Breitkreuts et al. extended the investigation of the kVAT technique and tried to individuate the optimal range of target sizes and depth treatable with the prototype of kVAT via Monte Carlo simulations [15]. The study investigates kVAT treatment for a total of 24 type of lesion, different for sizes (from 1 cm to 4 cm) and depths (superficial, middle, deep), in two homogeneous phantoms. Additionally, was investigated the kVAT delivery for two breast patients in prone and supine positions treated with a hypothetical PBI to a 4 cm and 3 cm lesions located approximately at 3 cm below the skin in the left breast.

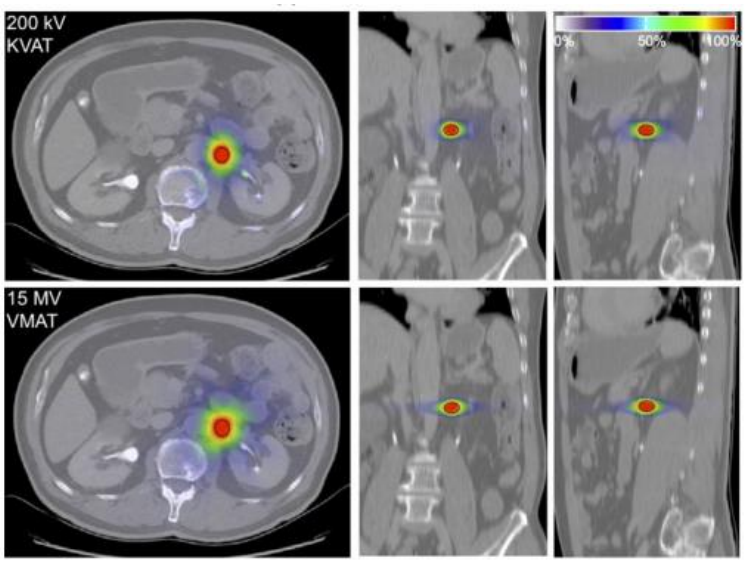

Figure 1.23 Comparison between isodose lines for 200 kV kVAT (top) and for 15 MV VMAT (bottom) treatments of the left pararenal lesion [14].

Patient phantoms were created using CT data of two female patients. Segmented prone breast image acquired on the dedicated breast scanner at UC Davis were converted to a virtual phantom, that was irradiate using a 360-degree arc treatment around the circumference of the breast with a source to axis distance of 34.4 cm.

To evaluate kVAT plans lesion-to-skin ratio (calculated as the ratio of the D_{95} divided by the mean dose delivered to a 2.4 cm x 2.4 cm x 2 mm volume in the centre of the beam at the surface of the patient) was used to determinate clinical acceptability. The authors justify this choice

asserting that the higher attenuation of kV radiation in superficial tissue typically renders the use of kV photons unacceptable for deep-seated lesions. Other considerations were performed using the metric of dose homogeneity (the ratio of the maximum dose and the minimum dose delivered to the lesion).

Figure 1.23 shows dose distribution for the case of the prone breast kVAT treatment; lesion-to-skin ratio and dose homogeneity were evaluated. This values are compared with dose distribution obtained with 6 MV photons treatment generated with Eclipse™ TPS (Varian Medical System, Palo Alto, CA, USA). Table 1.2 compares lesion-to-skin ratio and dose homogeneity between the prone kVAT treatment and 6 MV LINAC simulations. As we can see, the lesion-to-skin ratio is higher for 6 MV photons for both lesions, while the homogeneity value was slightly better.

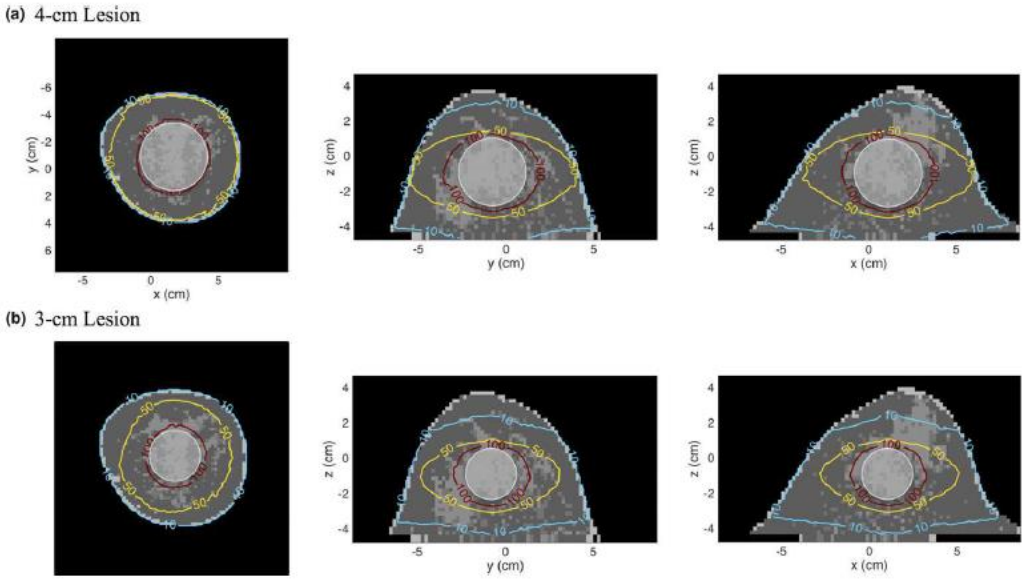

Figure 1.24 Dose distribution for the prone breast phantom treated with 360-degree kVAT in axial, sagittal, and coronal view (from the left side to right side) for the a) 4 cm lesion and the b) 3 cm lesion [15].

Case	Lesion-to-skin ratio	Dose homogeneity
4 cm, kVAT	2.3	1.43
4 cm, 6 MV LINAC	5.2	1.29
3 cm, kVAT	3.3	1.31
3 cm, 6 MV LINAC	6.9	1.31

Table 1.2. Calculated values of lesion-to-skin ratio and dose homogeneity for the 4 cm and 3 cm lesions in the prone breast patient treated with kVAT and 6 MV photons.

A comparison between prone and supine cases was also performed via MC simulations. This comparison showed that the prone orientation allows for more uniform coverage of the lesion while also spreading dose to healthy tissues maintaining the dose to the lesion.

The work of the Canadian group demonstrated that kVAT is suitable in the treatment of a variety of phantom cases and two breast cases. The best suited to the treatment of smaller lesions (1-2 cm in diameter) at depth down to 8.1 cm and moderate lesions of 3 cm diameter with larger arc angles at depth ranging from 3 cm to 8.1 cm. Future research will focus on optimization of this novel arcing kilovoltage x-ray radiotherapy system in order to evaluate additional clinical benefit.

Chapter 2
Monte Carlo simulations for the kV-EBRT technique

Basic goal of radiotherapy treatment is the irradiation of a target volume while minimizing the amount of radiation absorbed in healthy tissue. Due to the high level of accuracy required for dose calculations, a Monte Carlo code is essential to investigate the feasibility of this novel technique and a comprehensive validation of the code is needed.

The topic of this chapter is, firstly, to provide an overview of Geant4, the toolkit used to implement Monte Carlo (MC) simulations, with particular regard to the code utilized to perform simulations for the kV-EBRT technique. Simulations allowed to recreate the geometry of technique with a virtual cylindrical phantom, mimicking the pendulant breast, irradiated with both monoenergetic x-rays and different polychromatic spectra.

The MC code developments from the previous version adopted for the case of parallel synchrotron beam sources (Di Lillo et al., 2018 [16]) are outlined. 2D and 3D dose map distributions have been showed in this section. They were produced for several breast models and irradiation. The MC code was validated vs. literature data and, as well as, experimental measurements and the skin sparing effect was analysed.

2.1 Basics of Geant4 toolkit

Simulations for kV-EBRT were performed with Monte Carlo code based on Geant4 (Geometry And Tracking) toolkit (version 10.00) installed on a Ubuntu 16.04 64-bit Linux virtual machine system, with Intel® Core™ i7-4790 @3.6 GHz (8 threads[2]) with 19GB of dedicated RAM.

Geant4 is a simulation toolkit started in 1998 from two studies done independently at KEK (the High Energy Accelerator Research Organization) and CERN (Conseil Europeén pour la Recherche Nucléaire) for simulating the passage of particles through matter. It includes a completely range of functionality including tracking, geometry, physics models and hits [17] and was used in different application from particle physics (high energy physics) to medical physics applications (low energy physics), thanks to object-oriented technique and implemented C++ programming language.

The analysis and design process of Geant4 followed the object-oriented (OO) methodology: the organization of the class files includes, currently, 17 major categories, and each category

depends on the others. As shown in Figure 2.1, Geant4 categories have a hierarchical organization: at the bottom of the diagram are located the categories that provide the foundation of the toolkit, and then the others, in a one-directional flow of dependencies. At the base of whole software there is the category *global*, that accomplishes the system of unit, constant, numeric and random number handling. *Materials* and *particles* include the definition of the materials and particles to be used in the run. *Geometry* category has the task to define the geometry of the system, including the place of all volumes. The tracking particles and the physical process they undergo are described in two categories: *track* and *processes.* The first contains classes for tracks and steps, the second contains implementations of models of physical interactions. Above these *tracking* category manages the evolution of a track's state and undertakes to provide information in sensitive volumes for hits and digitisation. Over these the *event* category manages events in terms of their tracks and *run* manages collections
of events and detector. Finally, *readout* category allows the handling of ''pile-up''. Moreover, there are categories that use all above and connect to facilities outside the toolkit to provide visualization and user interface capabilities.
Each category contains classes and each class includes methods that are basic functions made accessible to the user and that can be called into simulation code.

2.2 Monte Carlo code

The MC code used was developed from a previous code used in the project funded by the INFN and proposed by Medical Physics group of Naples: SR^3T (Synchrotron Radiation Rotational Radiotherapy for Breast Cancer). In this previous version the code simulated the breast irradiation with monochromatic synchrotron radiation source adopting the same pendulant breast geometry proper in the kV-EBRT technique.
The whole code was based on low energy physics list Option4. The previous one was modified in many parts to adapt at the kV-EBRT. The previous simulated breast irradiation with parallel monochromatic beams produced by a synchrotron, on the other hand kV-EBRT adopts a cone x-ray beam. The x-ray beam was "electronically" collimated in order to irradiate a defined rectangular area at the isocentre of the system. The source rotated over a 360 degrees arc, in according to rotational radiotherapy. The rotation of the source was also implemented in the code.

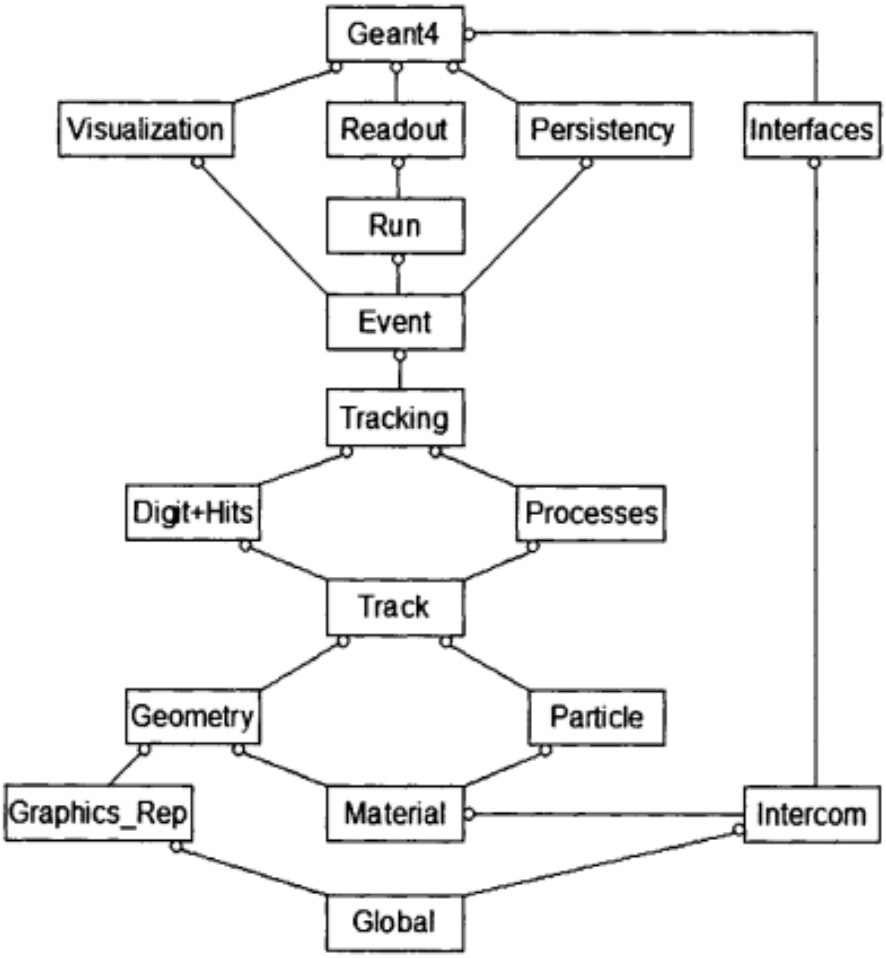

Figure 2.1 Category diagram of the Geant4 toolkit. This organization permits a better control of the code thanks to his clear hierarchical structure of domains [17].

2.2.1 Physics model

According the report of AAPM (Association of Physicist in Medicine) task group 195 (2015), the Option4 physics list was adopted, specifically for low energy physical processes. For kilovoltage x-ray beams the available processes include photoelectric effect, Compton scattering, Rayleigh scattering, bremsstrahlung, ionization.

PhysicList class retrieve all the physical processes that are involved in the interaction radiation-medium from photon cross section database of the XCOM library [16] of NIST.

In *PhysicList* class it is possible to define in addition to physical process, also the production thresholds.

Typically, in Geant4 applications, secondary particles were generated only above a given kinetic energy threshold, to save computational power. Threshold values for secondary particles

(principally delta rays) are defined in terms of the distance travelled by the particles in the medium and converted by Geant4 in terms of energy; only secondary particles with ranges greater than the cut-off range will be generated. Cut-off range were fixed as 1 mm for photons and 1 μm for electrons for all materials. The corresponding energy associated depends on material of the medium. For example, an electron range cut of 100 μm corresponds to 990 eV in air, 84.3 keV in water, 351.4 keV in tungsten [18].

Below these production thresholds the energy loss in the medium is calculated using *continuous slowing down approximation* with a maximum step of 100 μm.

2.2.2 Breast models and irradiation geometry

Typically, the term "geometry" in Geant4 refers to the volumes built in the simulation. A cylinder was used to model the pendulant breast, with a diameter of 14 cm (that corresponds to the breast of average diameter) and variable height. Different breast models were considered, each of these for a given type of material and cylinder size. The simulations assumed the phantom a continuous, non-voxelized object and homogeneous the materials selected for the cylinder: polyethylene and three type of breast composition of a given combination of glandularity (0% glandular, 50% glandular, 100% glandular) were investigated. Composition of breast tissue for each glandular fraction were obtained by weighting their elemental constituent (H, C, N, O, P) (see Table 2.1). The values of the attenuation and absorbed coefficient of the materials and compound, as well as their density, were derived from values of NIST database.

The chest wall was modelled as a box of water and was used to consider the scattered photons from the patient body.

Some breast models regarded the study of dose distribution in a breast with a small lesion. Lesion was modelled as a cylinder of 75% glandular composition (1.5 cm diameter and 2 cm tall) and were added into the primary phantom. The central axis of the hypothetical tumour was positioned at 1.75 cm and 7 cm from the cylinder edge to evaluate lesion-to-skin ratio for lesions at different depths.

The cone beam source in the code was an isotropic point source that could be rotated over 360 degrees in a circular orbit around the isocenter of the system in steps of 1 degree. The isocenter of the set-up was not fixed at central axis of the phantom, but it could be translating, if requested, in the x-y plane, to allow rotations around any axis. The isocenter axis was

coincident with the central axis of the breast or, in case of inhomogeneous phantoms model with the central axis of the lesion.

The source was "electronically" collimated in the horizontal and vertical plane: various beam size, as width and height at isocenter, were achieved in order to irradiate different portion of the breast. Beam width varied from 1 cm to 14 cm, when the breast was totally irradiated; beam height at isocenter was fixed to 0.1, 2 or 10 cm. The input parameters were:

- the width and height of the x-ray beam;
- diameter of the cylindrical phantom;
- height of the cylindrical phantom;
- mass energy-absorption coefficient of the material;
- density of the material;
- source to isocenter distance;
- degree angle of rotation.

Glandular Weight Fraction (%)	**Total tissue density (g/cm^3)**	**Hydrogen**	**Carbon**	**Nitrogen**	**Oxygen**	**Phosphorus**
0	0.9301	0.112	0.619	0.017	0.251	0.001
50	0.9819	0.107	0.401	0.025	0.464	0.003
75	1.0101	0.1045	0.293	0.0285	0.592	0.004
100	1.0400	0.102	0.184	0.032	0.677	0.005

Table 2.1 Weight fractions of elements and total tissue density as a function of glandular weight fraction.

Figure 2.2 shows a phantom shaped as cylinder of 14 cm diameter was placed at isocenter of the system (which in this case coincide with the central axis of cylinder) and was irradiated with an x-ray cone beam rotating 360°.

2.2.3 Polychromatic spectra implementation

Simulation were performed for both monochromatic and polychromatic x-ray beams. The making of polychromatic x-ray source was allowed by the creation of an algorithm, given as macro input to Geant4, starting from spectra produced by two different software: SpeckCalc [19] and TASMICS (Version 1.0). The first was a code that uses a graphical interface to perform a very fast x-ray spectrum calculation for tungsten targets bombarded by electrons until 300 kV. TASMICS is a tool used to produce tungsten anode x-ray spectrum with 1 keV energy resolution

from 60 keV to 640 keV. This data base of x-ray spectra is based on simulation in MCNPX 2.6.0.

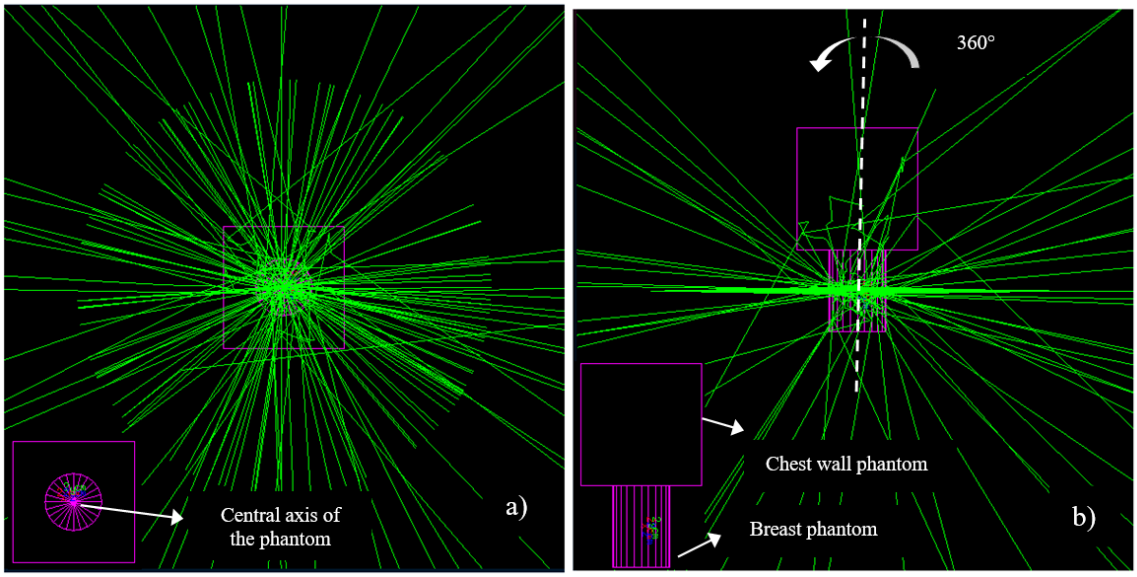

Figure 2.2 Implemented geometry in the Geant4 code to simulate the kV-EBRT treatment. The pendant breast was modelled as a cylindrical phantom placed at isocenter of the system and irradiated with an x-ray cone beam rotating 360 degrees around the central axis of the phantom. A polyethylene box modelled the chest wall. a) Axial view. b) Coronal view.

2.2.4 Dose scoring

MC simulations must score the physical quantity of interest in the breast models described previously. The previous code scored the energy deposited in the phantom produced by interactions of both primary and secondary photons (scattered photons, fluorescent, bremsstrahlung photons) during the interaction with material. The scored energy included the energy deposited in the material by the electrons produced in the photon hit. The energy deposited was scoring in eV unit. *EnergyDeposition* class was modified to obtain the absorbed dose in the phantom in mGy unit.

In addition, the event position was scored. The scoring resolution was varied in according to the simulated case: isotropic ($1 \times 1 \times 1$ mm^3) and anisotropic ($1 \times 1 \times 0.1$ mm^3) voxels were used. The simulation output was a three-dimensional dose map obtained associating the deposited energy by any interaction with the event position. Voxels dimensions had an influence on computation time of data analysis: with smaller voxels computational time grow from few hours to many hours.

2.2.5 Data analysis

The simulation output was stored as images in .txt format and represented dose distributions in axial slices of the phantom. Successive analysis was achieved with different software. Following step was image analysis through ImageJ 1.50b software (public domain, [20]). This software supported image stack reconstruction, with the creation of a macro, and permitted to obtain radial dose profile for all the simulations type. Finally, software Origin 9.0 64 bit [21] allowed generation of fits and graphics, while data handling and storage was achieved using Microsoft Excel 2016 [22].

2.3 Simulations with a monochromatic beam

Energy	178 keV
Material	Polyethylene
Phantom's dimensions	14 cm diameter, 9 cm height
Beam height at isocenter	1 mm
Beam width at isocenter	7 cm, 14 cm
Number of photons	10^6 for 1 cm horizontal collimation 10^8 for 14 cm horizontal collimation
Scoring resolution	$0.1 \times 0.1 \times 0.1$ cm^3
Distance source-to-isocenter	51.1 cm

Table 2.2 Characteristics of simulations performed with monochromatic x-ray beam at 178 keV.

Before keeping on with this work a validation of the code was required. First validation of the MC code was achieved matching ours and simulations found in literature.

As landmark simulations performed by Prionas et al. in their work about the feasibility of kV-EBRT [10] were chosen. For this purpose, our code reproduced the set up described in the study, as reported in Table 2.2.

A monochromatic x-ray source of 178 keV photons energy was set to irradiate a homogenous phantom with kV-EBRT technique. The phantom was a polyethylene (PE, density = 0.94 g/cm^3) cylinder with a diameter of 14 cm and 9 cm height. The point source performed a rotation of 360 degrees around the cylinder. Figure 2.3 shows implemented geometry: vertical beam collimation was fixed at 1 mm at isocenter and two simulations were achieved with 1 and 14 beam widths at isocenter. Simulations outputs were obtained by associating the energy absorbed

in the phantom to the deposited energy due to both primary photons and secondary particles with a scoring resolution of $0.1 \times 0.1 \times 0.1$ cm^3.

In order to produce radial dose profiles comparing with literature data, central slice of the phantom was analysed.

Validation of the code was performed comparing radial dose profiles with simulated dose distributions achieved by Prionas et al. in literature.

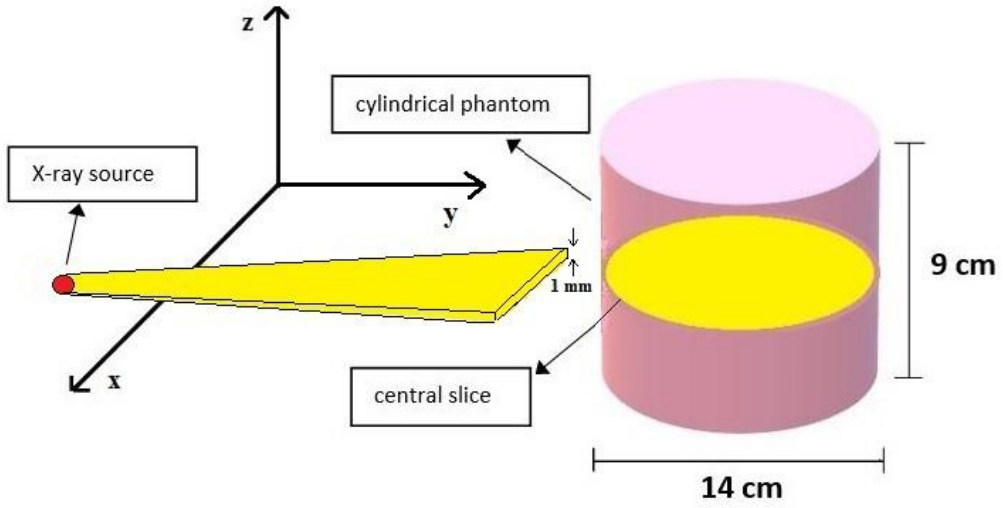

Figure 2.3 Geometry of simulations for the irradiation of the polyethylene phantom with a monochromatic photon beam of 178 keV.

	Central fit: $f(x) = P1x^3+P2x^2+P3x+P4$					**Tail fit: $f(x) = ax^b$**		
Collimation width	**P1**	**P2**	**P3**	**P4**	**R^2**	**a**	**b**	**R^2**
1 cm	-5.83E-09	4.61E-09	-1.18E-09	3.38E-09	1.000	1.30E-09	-1.18	0.979
14 cm	4.08E-13	-3.73E-13	4.95E-12	2.36E-10	0.996			

Table 2.3 Fitting function, function coefficients and goodness of fit for 1 and 14 cm collimation widths.

Table 2.3 reports function used for dose distribution fitting for the two different beam sizes, with functions coefficients and goodness of fit.

Radial dose distributions were extracted from fitting function data: Prionas proposed a third-grade polynomial to represent the inner cupped portion of dose deposition and a power function to describe dose tails extending radially outward.

Figure 2.4 shows a superposition between profiles for 14 and 1 cm horizontal collimation widths. For a 14 cm collimation, the central-to-periphery dose ratio is 0.63, where the expected

value is 0.64, with a percentage difference of 1.2%. At distance of 3.5 cm from the cylinder axis the percentage of central dose was 114.3%, where the expected value was 112.8%. On the other hand, for 1 cm collimation, the cylinder edge dose was less than 7% of the central dose deposition (the central dose value in the present analysis was always calculated at 1.34 mm from the isocenter), as expected from literature.

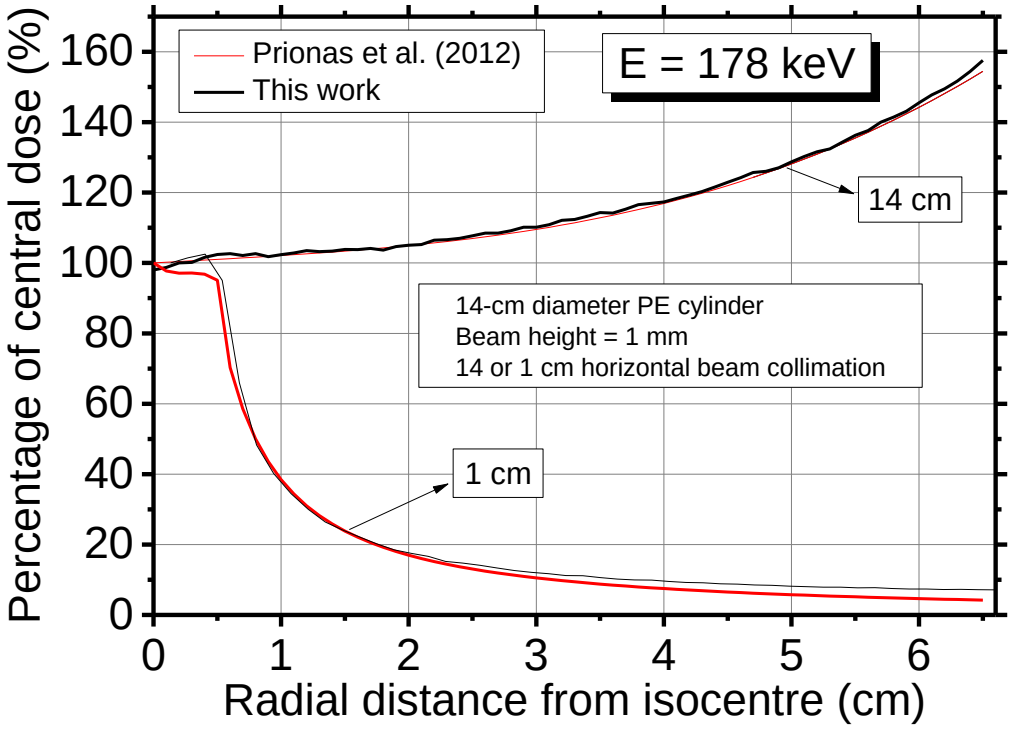

Figure 2.4 Comparison between monochromatic 178 keV simulations (for 1 or 14 cm horizontal beam collimation at the isocenter) and literature data for the same geometry and energy. Solid lines are referred to radial dose profile obtained from fitting function data provided by Prionas's work. Dash lines are referred to radial dose profile allowed from simulations performed in this thesis.

Good agreement was found between simulations obtained with our code and those found in literature with the same monochromatic beam and the geometry.

The process of validation includes other steps: in this work the validation of the code was achieved, moreover. Finally, the validation process was completed in the third chapter comparing experimental data of a previous work and measurements performed with an x-ray tube.

2.4 Simulations with a polychromatic beam

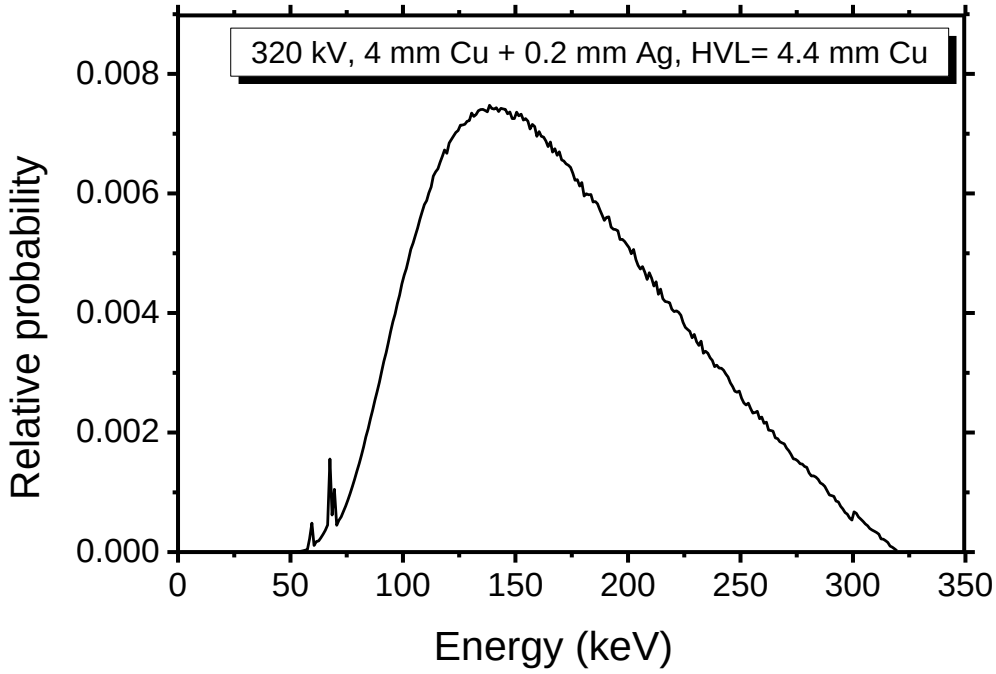

Figure 2.5 Polychromatic spectrum used for simulations: 320 x-ray beam filtered with 4 mm Cu and 0.2 mm Ag (half value layer 4.4 mm Cu) given by TASMICS tool. Energy resolution 1 keV. The image shows relative probability for x-ray photons on varying energies. Histogram was normalized so that, total probability was 1.

This paragraph presents simulations generated by irradiating a cylindrical breast model of 14 cm diameter and 20 cm tall irradiated, according to rotational kV-EBRT technique, with a 320 kVp x-ray spectrum.

For this purpose, x-ray beam was set on 320 kV with a 4 mm of Cu and 0.2 mm Ag filtration (HVL= 4.4 mm Cu). The 320 kVp spectrum was generated with 1 keV energy bins through TASMICS tool and used as macro input for Geant4 code. This energy was selected to obtain the same polychromatic beam used by Prionas [10] and, as well as, this choice was based on the availability on the market of kV tungsten anode orthovoltage tubes, as suggested by Prionas. Figure 2.5 shows polychromatic spectrum used.

Simulations with a variety of geometrical set-ups, beam sizes, and materials were performed in order to investigate the novel rotational RT for breast cancer and as well as to achieve a further validation of the Geant4 code.

2.4.1 Simulations at 320 kV in homogenous phantom

Energy spectrum	320 kV
Half value layer	4.4 mm Cu
Materials	Polyethylene
Phantom's dimensions	14 cm diameter, 20 cm height
Beam height at isocenter	2 cm
Beam width at isocenter	1.5 cm, 3 cm, 5 cm, 7 cm, 9 cm, 12 cm, 14 cm
Number of photons	10^8 for all type of simulations
Scoring resolution	$0.1 \times 0.1 \times 0.1$ cm^3
Distance source-to-isocenter	51.1 cm

Table 2.4 Characteristics of simulations performed with polychromatic x-ray beam of 320 kV in a homogenous PE cylinder placed at isocenter of the system.

In this section MC code was employed to investigate the irradiation of the homogenous cylinder with an x-ray beam rotating around the isocenter for a complete rotation of 360 degrees. The central axis of the cylinder was coincident with the isocenter of the system. Based on its similar x-ray attenuation properties compared to adipose tissue, polyethylene was chosen as material of the phantom.

Different simulations were achieved varying beam size in the horizontal plane (from 1.5 cm to 14 cm), while beam size in the vertical plane was set at 2 cm. In Table 2.4 are summarized the setting parameters for these simulations.

In order to carry out a qualitative analysis, 2D and 3D maps of dose distribution in the phantom are achieved. Figure 2.6 shows 2D and 3D dose distributions achieved into an image obtained as summation of the slices irradiated by the x-ray beam for different values of collimation in the horizontal plane.

In Fig.2.6 a) dose values are in mGy and are displayed in grey scale, in axial view. For narrow beam simulations a peaked profile is achieved: for 1.5 cm beam width dose values change from 1.2×10^{-10} mGy per photon, near the central axis of the cylinder, to 0.1×10^{-10} mGy per photon on the edge with a rapid fall off. Dose decrease was about 92% for 1.5 cm beam width, while was 49% for 7 cm beam width (central dose was about 2.9×10^{-10} when the edge was 1.5×10^{-10} dose). On the contrary, broad beam geometry produces a cup-shaped profile

with maximum dose deposition on the edge of the slices directly irradiated by the beams. The shape of dose distribution changes a lot with horizontal beam collimation.

In Fig. 2.6 b) 3D dose distributions for 1.5 cm and 14 cm beam width show a focused distribution in the centre with a rapid exponentially decrease on the edge and a biconcave distribution with a totally cup-shaped profile, respectively. Intermediate cases resulted in a hybrid saucer-shaped dose distribution.

A quantitative analysis was also performed to evaluate the skin sparing effect for different horizontal beam collimations. Figure 2.7 shows dose profiles in terms of percentage of central dose (the ratio between radial dose divided for the value of central dose) versus distance from cylinder axis.

It is possible to see in Fig. 2.7 edge dose values achieved for each beam width increased as was widened collimation in the horizontal plane. The edge dose varied from about 10% of the maximum dose deposition (that was achieved at distance zero from the cylinder axis) for 1.5 cm beam width to about 140% for a totally irradiation of the phantom (14 cm beam width).

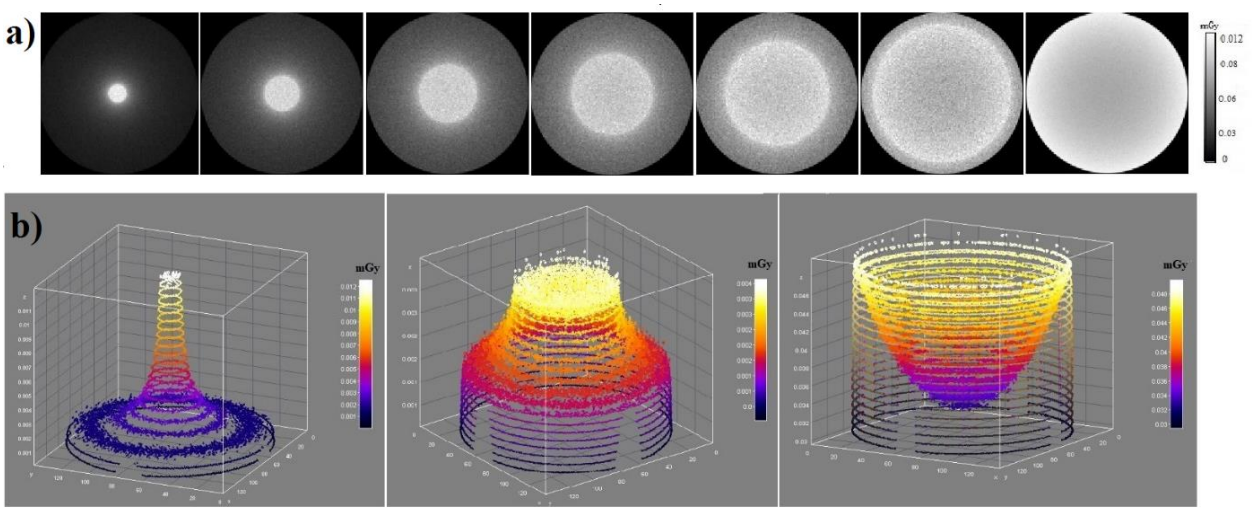

Figure 2.6 a) 2D dose distribution in the center of a cylindrical phantom (14 cm × 20 cm) for different values of collimation in the horizontal plane (1.5, 3, 5, 7, 9, 12, 14 cm, respectively from the left side to right side) and 2 cm collimation in the vertical plane. b) 3D isodose lines for 1.5, 7, 14 cm beam width (from the left side to right side). Tube voltage: 320 kV, half value layer 4.4 mm Cu.

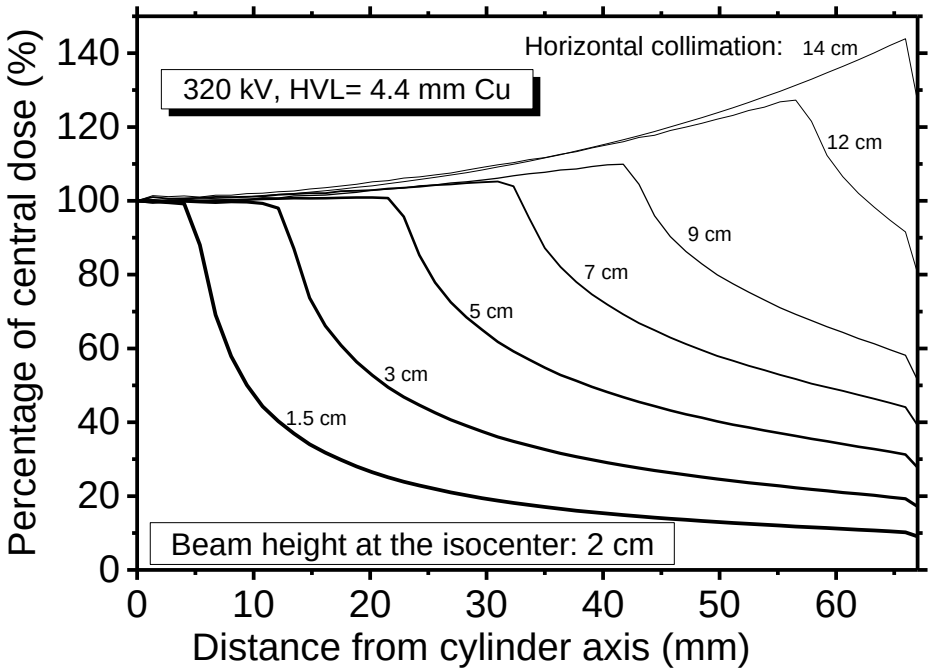

Figure 2.7 Radial dose profile (expressed as percentage of the central value, versus the radial distance in the phantom) in a 14 cm diameter PE cylindrical phantom for different beam width. It is possible see the inversion of the radial dose profile from a cup-shaped profile with high edge dose (about 140% of the central dose for 14 cm horizontal collimation) to a peaked profile with low edge dose (about 10% of the central dose for 1.5 cm horizontal collimation).

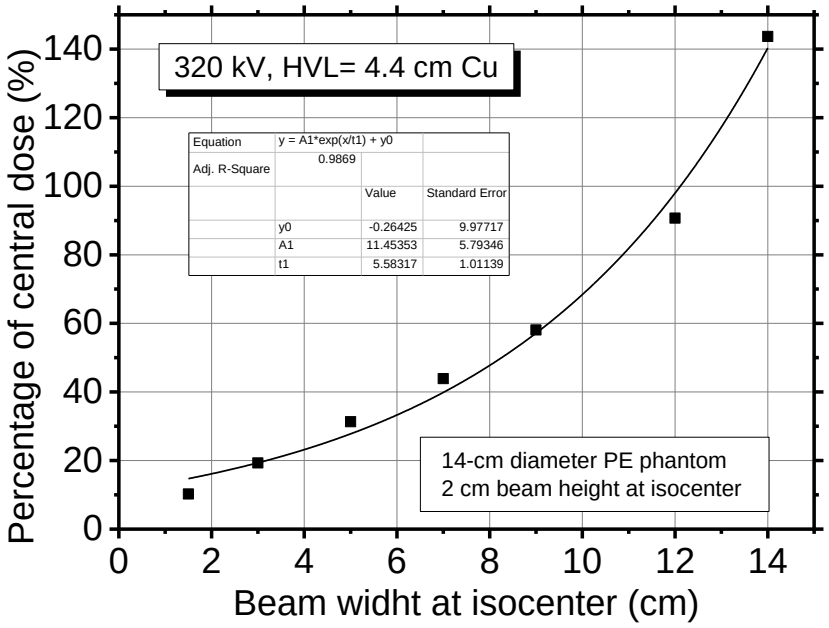

Figure 2.8 Variation of percentage of central dose at edge of the PE cylindrical phantom for different collimation widths at isocenter in the horizontal plane. Black line describes an exponential growth of the percentage edge-to-center dose ratio with the beam width at isocenter.

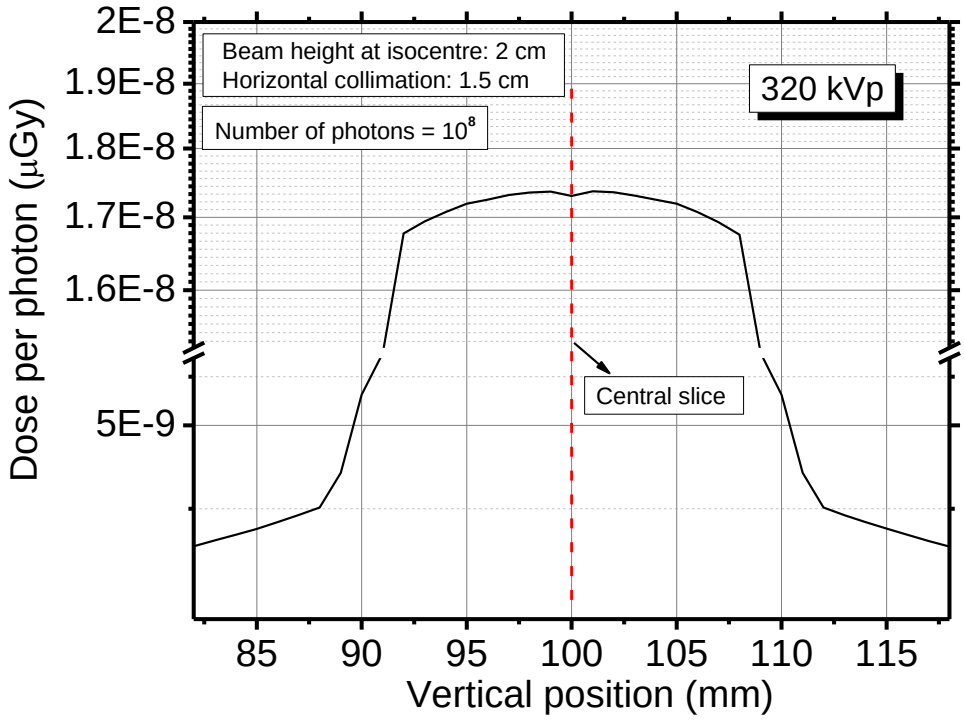

Figure 2.9 Vertical dose spread profile for 1.5 cm beam width at isocenter.

Figure 2.8 shows the trend of values of percentage of central dose at edge of the phantom for different collimation widths in the horizontal plane when beam height was fixed at 2 cm.

As shown by a 1.5 cm beam delivering of about 10% of the maximal dose deposition to the perphery, small volumes can be treated with the beast skin receiving a small fraction of the dose. The influence of the scattered photon interactions was evaluated along the vertical axis of the phantom. Figure 2.9 shows vertical dose spread profile for 1.5 cm beam width in terms of dose per photon (μGy) versus vertical position along the cylinder axis.

Limited influence of scatter dose at distance of 10 mm from the central slice was observed: dose per photon decrease from 1.7 Gy per photon to 6.4×10^{-12} Gy per photon.

2.4.2 Simulations at 320 kVp in a tumor phantom

The feasibility of PBI with the kV-EBRT technique was studied by performing MC simulations with a non-homogenous phantom. However, limitations due to acceptable skin sparing restrict the size of treatable lesions with this new technique.

Simulations at 320 kVp in the homogenous phantom for different beam size allowed dose distributions that depended strictly on beam collimation in the horizontal plane.

Energy spectrum	320 kVp
Half value layer	4.4 mm Cu
Materials	50% glandular, 0% glandular, 100% glandular
Phantom dimensions	14 cm diameter, 20 cm height
Beam size at isocenter	1.5 × 2.0 cm^2 (W × H)
Number of photons	10^8 for all types of simulations
Scoring resolution	0.1 × 0.1 × 0.1 cm^3
Source-to-isocenter distance	51.1 cm

Table 2.5 Characteristics of simulations performed with polychromatic x-ray beam of 320 kV irradiating a cylinder of different glandular composition with a small lesion of 75% glandular fraction placed at different depths from the cylinder axis.

In order to achieve the irradiation of a target volume, minimizing the amount of radiation to the skin, a focused dose distribution was required. PBI was achievable even if the irradiated area is sufficiently restricted. This means that only small target can be treated with kV-EBRT.

To study PBI with kV-EBRT different simulations were performed. Breast was modelled as a cylinder (14 cm diameter and 20 cm tall) of different glandular fraction.

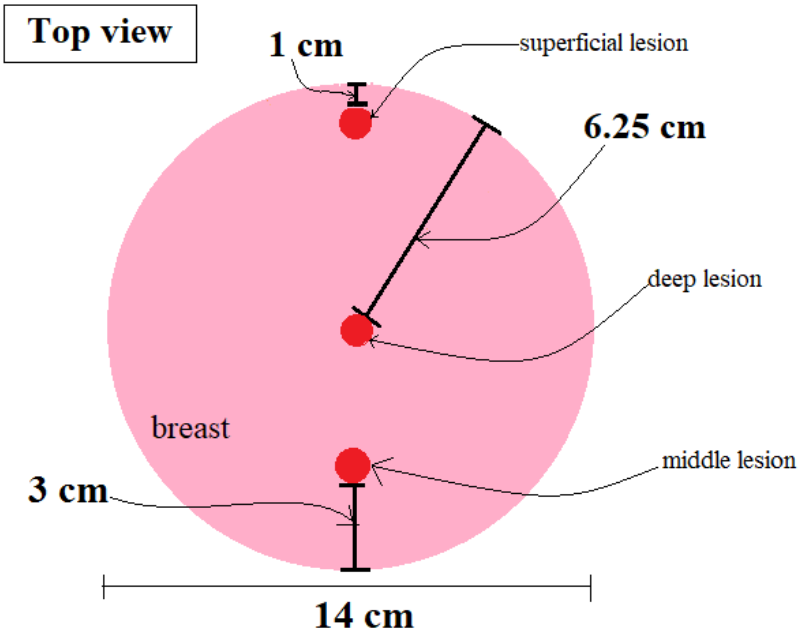

Figure 2.10 Illustration of lesions of 75% glandular tissue in a 14 cm diameter cylindrical phantom, mimicking the pendulant breast. The lesions were modelled as a cylinder of 1.5 cm diameter and 2 cm tall and were positioned at two different depths in the breast phantom: the superficial lesion is placed at 1 cm from the edge and the deep lesion at 6.25 cm. Frontal view.

	Deep lesion	Middle lesion	Superficial lesion
Target size	1.5 cm diameter, 2.0 cm tall	1.5 cm diameter, 2.0 cm tall	1.5 cm diameter, 2.0 cm tall
Target material	75% glandular fraction	75% glandular fraction	75% glandular fraction
Skin-to-isocentre distance	7 cm	3.75 cm	1.75 cm

Table 2.6 Characteristic of targets implemented in the MC simulations.

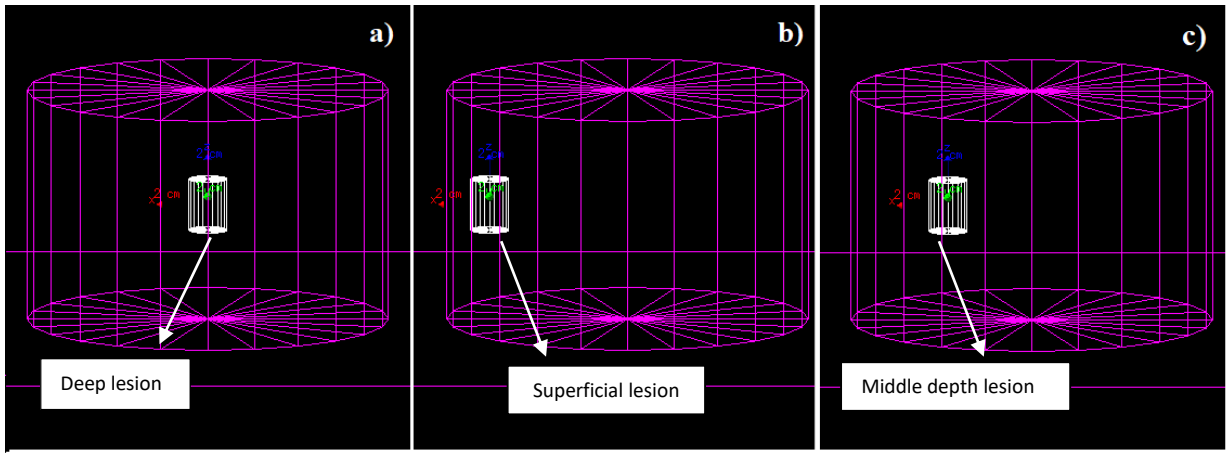

Figure 2.11 Side view of the geometry implemented in the MC code to simulate the kV-EBRT treatment for a phantom breast (14 cm diameter, 20 cm tall) with a small lesion (1.5 diameter, 2.0 cm tall) placed in two different positions: a) deep lesion, at 6.25 cm from the cylinder edge. b) superficial lesion at 1 cm from the cylinder edge.

Previous study (seen in 2.4.2 section) about dose distributions in the homogeneous PE phantom indicated that for 1.5 cm beam width the percentage of central dose at the edge of the cylinder was about 10%. This means that only the 10% of the central dose value was absorbed by the skin of patient. For this reason, the target was modelled as a small cylinder of 1.5 cm diameter and 2 cm tall. The material of target was set on 75% glandular composition for all type of simulations. Table 2.5 summarize the set values for these MC simulations.

Three different for depths from the central axis of the breast, were investigated: a deep lesion, coincident with the central axis of the cylindrical breast phantom, a middle depth placed and a superficial lesion, placed respectively at 3 cm and 1 cm from the edge of the cylindrical phantom mimicking the breast.

Positions of the targets respect the breast surface is show in Figure 2.10 and summarized in Table 2.5. In Figure 2.11 are shown the geometry modelled in the simulations.

The targets were irradiated with the 320 kVp x-ray beam rotating in a circular orbit of 360 degrees and beam collimation at the rotation axis was fixed at 1.5 cm × 2.0 cm. The center of rotation corresponding to the tumour position in all the MC simulations.

2D dose distributions were evaluated in the irradiated slices for different breast models (50% glandular fraction, 100% glandular fraction; 0% glandular fraction) and dose distributions with the three different placed targets were indagated.

Radial dose profiles were achieved in a cylinder of 14 cm, 3.75 cm and 1.75 cm diameter and 2.0 cm tall for the three types of lesion.

Radial profiles and 3D dose map show, as the previous case of homogenous phantom, a focused dose profile in the irradiated volume with the maximal dose deposition on target volume with low edge dose values (Figure 2.12).

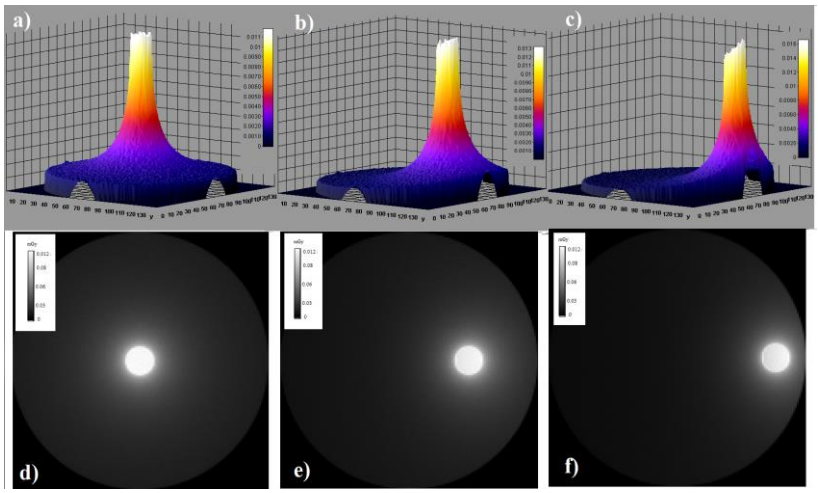

Figure 2.12 3D and 2D dose maps obtained from MC simulations of 50% glandular breast with a small lesion (1.5 cm diameter, 2.0 cm tall) irradiated with a 320 kV spectra. 3D distributions are shown in false colour from blu (low dose values) to white (high dose values) for simulation with a) a deep lesion, b) a middle depth lesion. c) superficial lesion. Two-dimensional maps in axial view show dose (mGy) distribution in grey scale (grey indicate low dose to phantom; white colour indicate high dose to the phantom) for simulation with d) a deep lesion, e) a middle depth lesion, f) superficial lesion.

Analysis of dose distributions in the volumes of interest (VOIs) were performed and lesion-to-skin ratio was used as a measure of the acceptability for dose to skin during the treatment of target at different depth in breast.

Figure 2.13, 2.14, 2.15 show 2D dose map in: a) axial, b) sagittal, c) coronal view, d) horizontal profile in the central slice of the phantom and e) vertical profile along the slices

directly irradiated by the beam. For the case of deep lesion, the principle of dose summation along the axis of rotation produced a dose distribution peaked at the centre of rotation for this area, which is narrower than in the WBI. For the case of off centre tumor the maximum of dose deposition not occurs at the centre of rotation but few millimetres from the previous one.

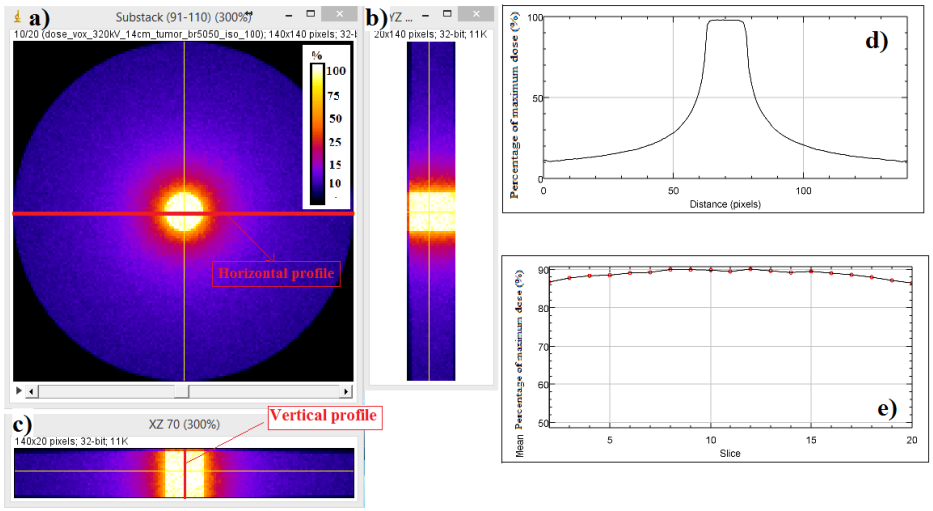

Figure 2.13 2D dose map at the mid-plane in the 14-cm diameter PE phantom obtained in WBI of a lesion placed at 7 cm from the surface phantom. The pixel values are in mGy normalized to the maximum value of dose. a) axial view. b) sagittal view. c) coronal view. On the right side are shown: d) Radial profile along the horizontal plane. e) Vertical profile along the rotation axis.

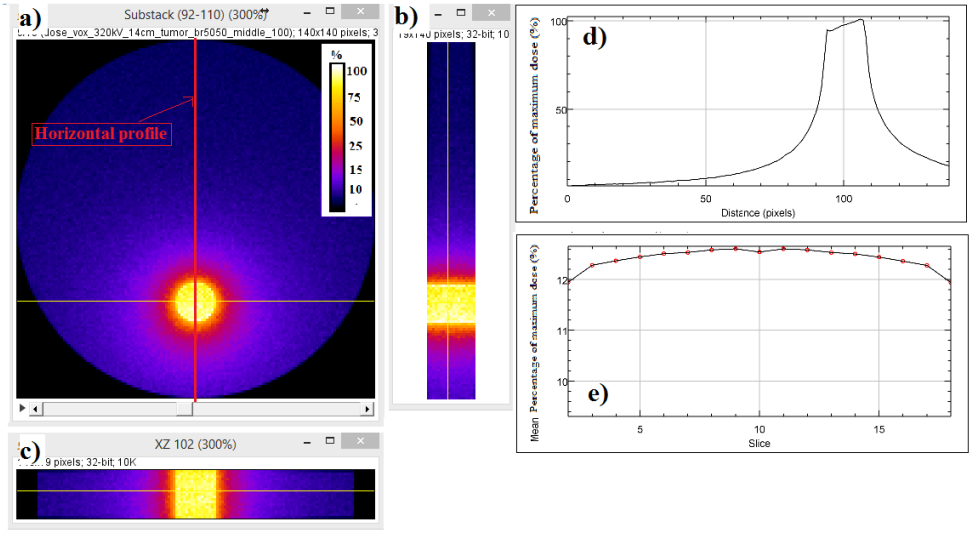

Figure 2.14 2D dose map at the mid-plane in the 14-cm diameter PE phantom obtained in WBI of a lesion placed at 3.75 cm from the surface phantom. The pixel values are in mGy normalized to the maximum value of dose. a) axial view. b) sagittal view. c) coronal view. On the right side are shown: d) Radial profile along the horizontal plane. e) Vertical profile along the rotation axis.

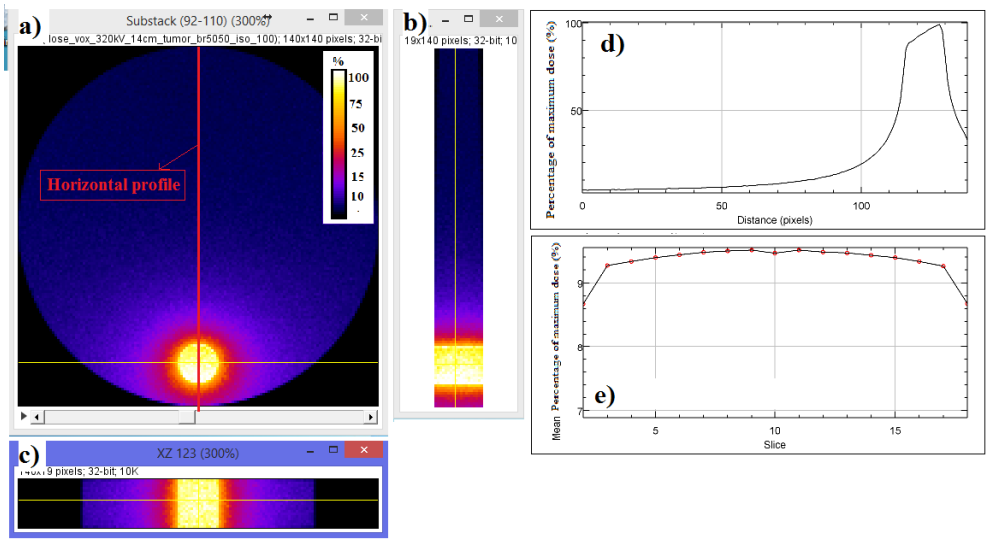

Figure 2.15 2D dose map at the mid-plane in the 14-cm diameter PE phantom obtained in WBI of a lesion placed at 3.75 cm from the surface phantom. The pixel values are in mGy normalized to the maximum value of dose. a) axial view. b) sagittal view. c) coronal view. On the right side are shown: d) Radial profile along the horizontal plane. e) Vertical profile along the rotation axis.

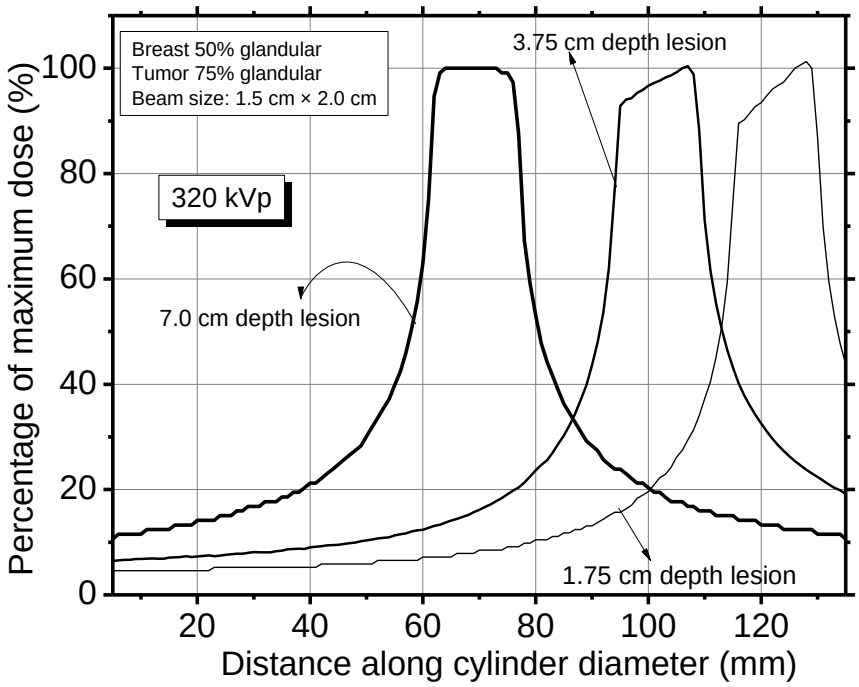

Figure 2.16 2D dose profiles achieved from images a) shown in figure 2.13, 2.14, 2.15. Selection was made from the left to the right (horizontal position) of those image that represent dose distribution correspondent to the irradiation with a 320 kVp x-ray beam (collimation: 1.5 × 2.0 cm^2 at the isocenter) of a 14 cm diameter breast phantom of 50% glandular tissue with three types of lesion (at 7.0 cm, 3.75, 1.75 cm of depths respect the edge of the breast).

Breast glandular weight fraction	Dose to target (μGy/photon) × 10^{-7}	Dose to skin (μGy/photon) × 10^{-8}	Lesion-to-skin-ratio (%)
50% glandular	1.12 ±0.01	1.218 ± 0.004	10.6
100% glandular	1.10 ± 0.01	1.260 ± 0.003	11.3
0% glandular	1.2 ± 0.03	1.282 ± 0.003	10.8

Table 2.7 Dose to target, dose to skin and lesion-to-skin ratio values for a deep lesion placed at central axis of the breast (1.5 diameter, 2.0 cm tall) for different values of glandular weight fraction. The lesion consisting of 75% glandular fraction.

Breast glandular weight fraction	Dose to the target (μGy/photon) × 10^{-7}	Dose to skin (μGy/photon) × 10^{-8}	Lesion-to-skin-ratio (%)
50% glandular	1.27 ± 0.02	2.040 ± 0.008	16.4
100% glandular	1.22 ± 0.02	2.171 ± 0.005	17.0
0% glandular	1.31 ± 0.01	2.210 ± 0.003	16.6

Table 2.8 Dose to target, dose to skin and lesion-to-skin ratio values for a middle depth placed lesion at 3 cm from the edge of the breast (1.5 diameter, 2.0 cm tall) for different values of glandular weight fraction. The lesion consisting of 75% glandular fraction.

Breast glandular weight fraction	Dose to the target (μGy/photon) × 10^{-7}	Dose to skin (μGy/photon) × 10^{-8}	Lesion-to-skin-ratio (%)
50% glandular	1.50 ± 0.001	5.121 ± 0.007	34.4
100% glandular	1.47 ± 0.002	5.080 ± 0.005	34.5
0% glandular	1.53 ± 0.002	5.311 ± 0.003	34.2

Table 2.9 Dose to target, dose to skin and lesion-to-skin ratio values for a superficial lesion placed at 1 cm from the edge of the breast (1.5 diameter, 2.0 cm tall) for different values of glandular weight fraction. The lesion consisting of 75% glandular fraction.

Table 2.7, 2.8 and 2.9 display the calculated values of mean dose to target and lesion-to skin-ratio, respectively for the case of deep lesion. middle depth lesion and superficial lesion. The percentage values of lesion-to-skin lesion for the case of deep target range between 10.6 – 11.3 and the highest skin sparing was found in the case breast 50% glandular.
Lesion-to-skin ratio was about 37% for the case of superficial lesion and ranges between 16.4-17 % for a middle target placed.

A quantitative analysis was performed selecting profiles from left to the right in the horizontal position of the image a) of the Figure 2.13 and from top to bottom of the images a)

of the Figure 2.14, Figure 2.15 that represent 2D dose distribution correspondent, respectively to the irradiation of a deep lesion, middle placed and superficial lesion in a breast of 50% glandular fraction.

Dose profiles were plotted and normalized to their maximum. As shown in Figure 2.16 the maximum dose deposit for the breast with a deep lesion occurs at the centre of rotation, then the maximum percent of dose decrease with an exponential rate. At the edge occurs about the 11% of the maximum dose. The dose decreases from the center (at 7 cm) to the edge (at 14 cm) of about 90% was observed, maximum dose was achieved in the target.

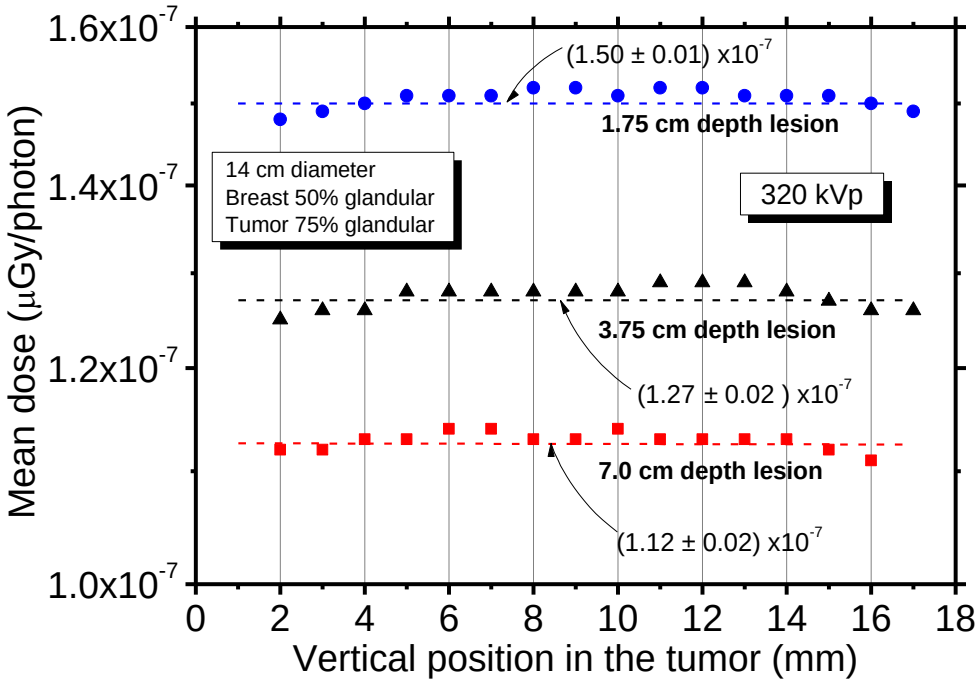

Figure 2. 17 Vertical spread profile of mean dose (µGy/photon) as function of vertical position in the target. The dash lines represent the mean values.

For the middle deep lesion and the superficial lesion, the maximum of dose deposit not occurs at the center of rotation but at 4.5 mm from the central axis of the target. At 13.5 cm, in the right side of phantom, occurs about the 20% and the 43% of the maximal dose deposit.

Dose homogeneity in the target volume was evaluated along the vertical position (figure 2.17). Vertical spread profiles allowed a mean dose homogeneity of 1.02 for all the case of interest.

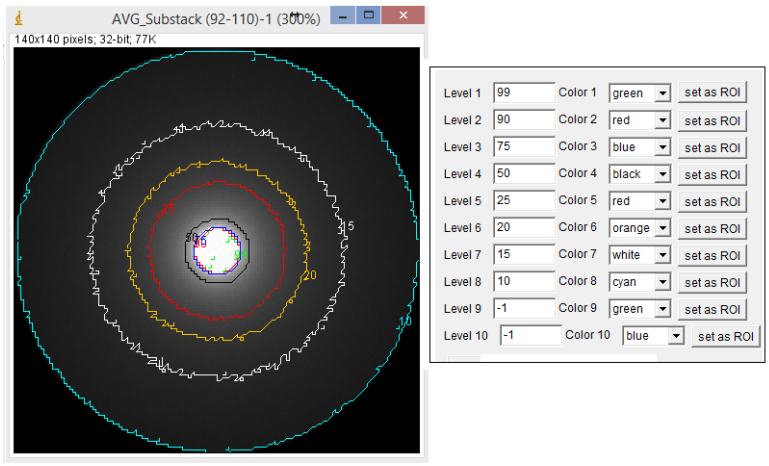

Figure 2.18 Isodose lines of the 2D map for a breast phantom of 50% glandular fraction with a lesion positioned at 7 cm from the edge.

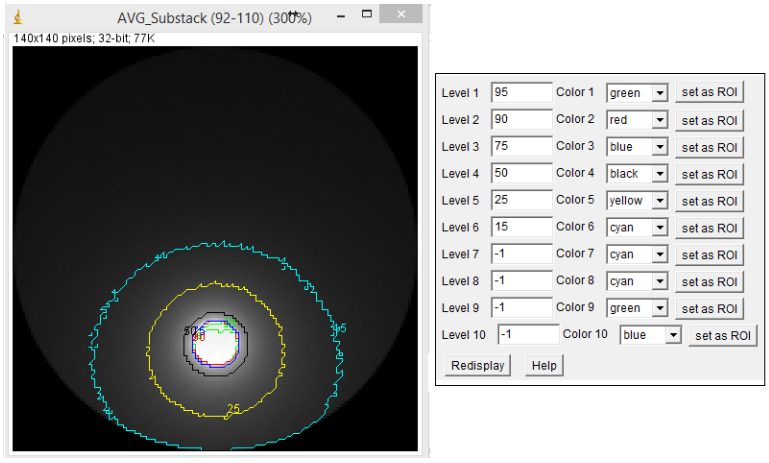

Figure 2.19 Isodose lines of the 2D map for a breast phantom of 50% glandular fraction with a lesion positioned at 3.75 cm from the edge.

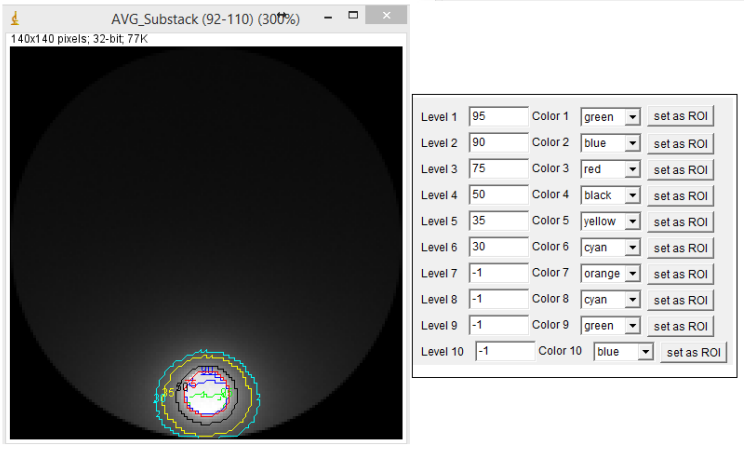

Figure 2.20 Isodose lines of the 2D map for a breast phantom of 50% glandular fraction with a lesion positioned at 1.75 cm from the edge.

Figure 18,19 and 20 show isodose lines evaluated in the 2D maps of the irradiated slices of the breast phantom. Pixel values are in mGy normalized to the maximum dose deposit value. Lines are in distinct colours to indicate the area with the same value of percentage of maximal dose deposition.

Study of dose distribution in superficial targets in breast phantoms of different compositions irradiated with the kV-EBRT technique show, a surplus of dose to the skin patient. On the contrary, a good skin sparing was achieved in all simulations with the deep lesion: the lesion-to-skin ratio was at most the 11.0% of the target dose.

To reduce dose to cylinder edge in the treatment of the superficial target another structure was implemented in the MC simulations: a *bolus* was added the surface of the breast.

Bolus is a "non-real" structure of tissue equivalent material, typically used in the TPS for the conventional RT. Normally *bolus* was simulated directly on the skin surface to even out the irregular patient contour and thereby provide a flat surface for normal beam incidence. The use of bolus was largely diffused in conventional radiotherapy treatment to ensure an optimal conformity and homogeneity of dose to the target.

In this work a *bolus* was modelled as a circular crown of the same material as the breast phantom (Figure 2.21).

The role of the *bolus* was hardening the kilovoltage beam, removing photons of low energy that deposit dose at the surface near the tumor location. In figure is shown the simulated geometry with a bolus of 5 width and 2 cm tall with an angular opening of 30 degrees directly placed on cylinder surface. Simulation with this bolus show a decrease of the lesion-to skin ratio for the case of breast with the 1.75 cm lesion. The lesion-to-ratio decrease from 34.2% to 29%.

This preliminary study indicates that is possible to treat even superficial lesion, near the skin surface, if the treatment provides the use of a bolus opportunely calculated to reduce dose to skin, so assuring skin sparing.

Future studies are demanded to optimize the implementation of the *bolus* structure and materials for superficial lesion treatment with the kV-EBRT technique.

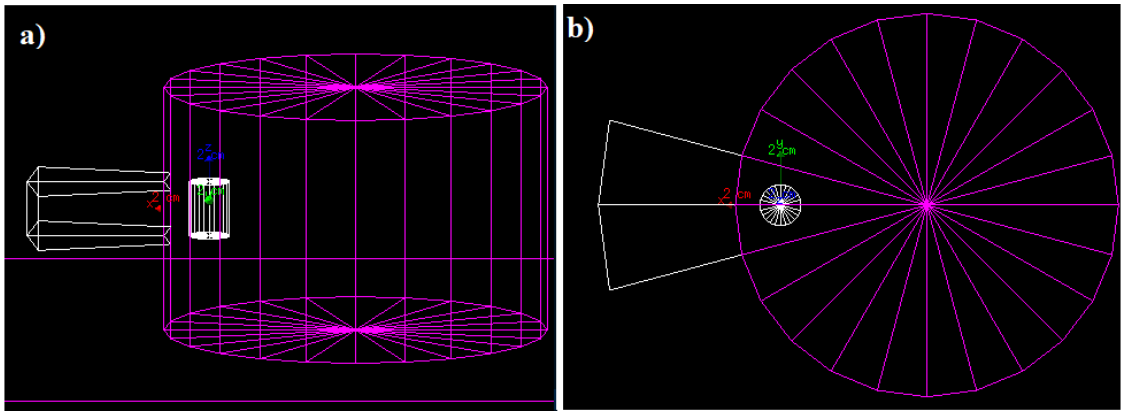

Figure 2.21 Geometry implemented in the MC code to simulate the kV-EBRT treatment of a lesion (1.5 cm diameter and 2 cm tall) placed at 1.75 cm from the breast surface with a bolus (5 cm width and 2 cm height) placed directely on the edge of the breast phantom. a) Side view. b) Top view.

Chapter 3
Experimental validation of the MC code

In MC study the experimental validation of the code was necessary. For this purpose, experimental measurements were achieved using a kilovoltage x-ray tube available in Medical Physics laboratory in Physics department at Federico II University.

The aim of this chapter is to describe the experimental set-up and the methods used to perform measurements with the kV-EBRT technique. The same geometry and energy spectrum was implemented in the MC code to compare measured radial dose profiles with simulations.

Furthermore, another validation was accomplished matching simulations results with experimental measurements achieved in a previous work [24].

3.1 Experimental set-up

The experiment was conducted at the Medical Physics laboratory of the University of Naples Federico II. The experimental data were acquired with a bench-top prototype of high resolution bCT scanner, which include a micro focus x-ray source, a CMOS flat panel detector, and stepper motors for vertical, horizontal motion and for gantry rotation. The x-ray tube used was a Hamamatsu L8121-03. General specifications of the x-ray tube are shown in Figure 3.1. By a graphical user interface is possible to set different parameters, moving the system along the three axis and rotate the entire gantry of any angle.

Parameter	Value	Unit
Tube Voltage operational range	40 to 150	kV
Tube Current operational range (large spot mode)	10 to 500	µA
Maximum output (large spot mode)	75	W
X-ray beam angle (coned)	43	degrees
Focus to object distance	17	mm
Operation	Continuous	-

Figure 3.1 Characteristic of the x-ray tube Hamamatsu L8121-03. On the left side is shown the tube and the x-ray control unit (http://www.hamamatsu.com).

The ionization chamber which is been used is a PTW Semiflex Type 31010 (Figure 3.2), a fully guarded cylindrical chamber commonly used in absolute dosimetry in radiotherapy, with

a 0.125 cm^3 sensitive volume, vented to air, waterproof. The nominal response is 3.3 nC/Gy and the maximum chamber voltage is ± 500 V. The sensitive volume has radius 2.75 mm and length 6.5 mm. The wall of the sensitive volume was made of 0.55 mm of PMMA and 0.15 mm of graphite, as is possible to seen in a radiography of the chamber (Figure 3.3).

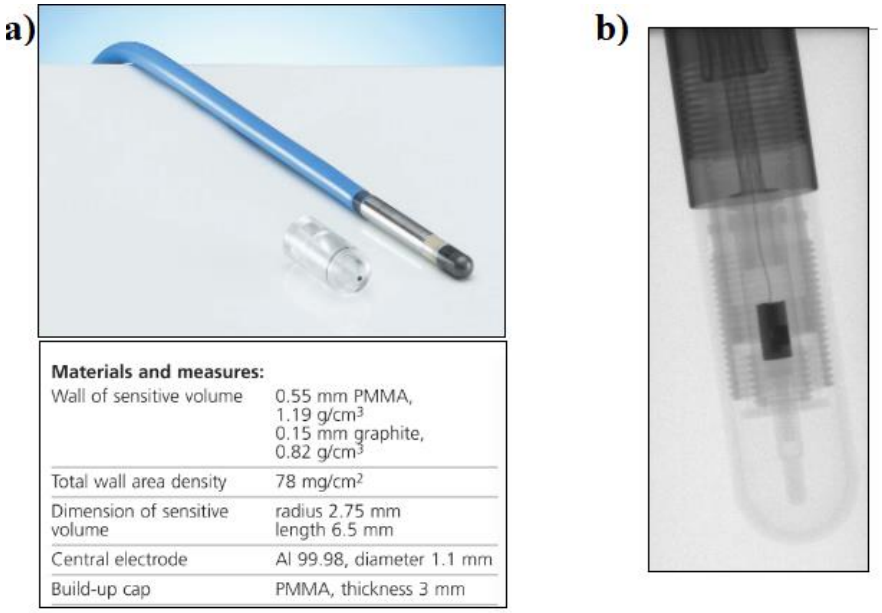

Figure 3.2 a) PTW Semiflex type ionization chamber and his characteristics [25]. b) Radiography of the Semiflex chamber put into the phantom central hole. Acquisition at 500 kVp, 500µA.

The electrometer used for the measurements is the UNIDOSE® E (PTW, Freiburg, Germany) (Figure 3.4). The electrometer and the ionization chamber have been both calibrated measuring absorbed dose to water D_w in a Co^{60} beam at temperature $T_0 = 20^0$ and pressure P_0 = 1013.25 hPa. The detector calibration factory was $N_{D,W}= 3.118 \times 10^8$ Gy/C. To give the dose in water as output, according to the IAEA protocol, the electrometer give the dose as product of the charge C measured for $N_{D,W}$:

$$D_w = C \cdot N_{D,W}$$

Furthermore, D_w measured must be correct for the temperature and pression at the time of measurements with a TPF (temperature and pressure correction factor):

$$TCF = \frac{(273.15 + T(°C))}{(273.15 + T_0)} * \frac{P_0}{P\ (mbar)}$$

Ionization chamber was inserted in a holed polyethylene cylindrical phantom of 14 cm diameter and 15 cm tall, to mimicking the breast (Figure 3.3). PE was largely utilized as material for breast phantoms because of their similar to adipose tissue attenuation characteristic (0.9325 g/ml vs 0.90 g/ml of adipose tissue). The holes of 1.3 cm were sited in different position to achieve dose measure at different depths in the phantom, as shown in Figure 3.4. Hole were placed at 0, 1.91, 3.18, 4.45 cm from the cylinder central axis.

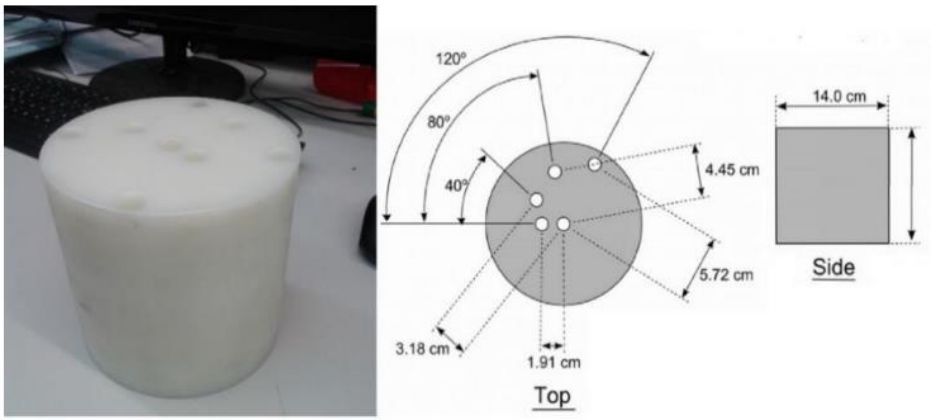

Figure 3.3 PE phantom holed at different distance from the center. Image on the left shows, in detail, positions of the holes and dimensions of the phantom.

During the irradiation the unutilized holes were filled by a PE cap. The hole correspondent to the point of measure was not filled to permit the insertion of the ionization chamber through a hollow PE cup.

Radiochromic films XR-QA2 (Gafchromic^{TM}, ISP-International Specialty Products Inc., Wayne, NJ) were used for measurements (Figure 3.4). They consist in one or double layer of radiation-sensitive organic microcrystal monomers on a thin polyester base with a transparent coating. After irradiation film colour change into blue and study of darkness in red channel carry out information about absorbed dose or beam shape. XR-QA2 are typically used for quality assurance in radiology applications. In this work they were not used as dosimeters, but just to fulfil a good system positioning and to assures a correct size of the x-ray beam at isocenter.

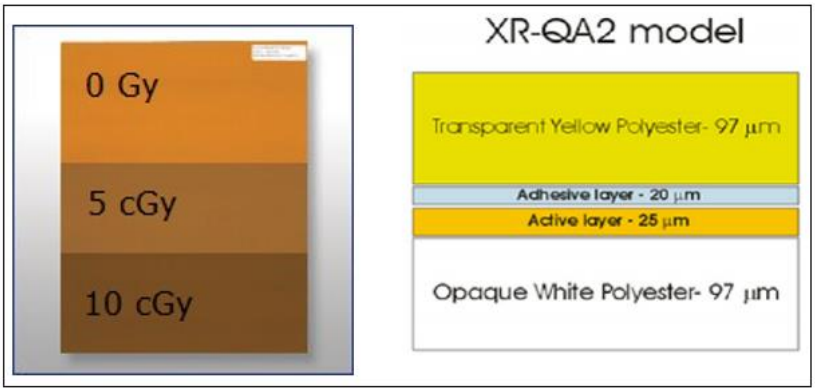

Figure 3.4 Gafchromic XR-QA2 model. On the left is shown the structure of the films. The yellow layer of polyester in expose to radiation. Last layer, of opaque white polyester, has a support function. The active layer of 25 µm of thichness exposed to irradiation turn its colour into blue. On the right is shown as the film changes colour for different irradiation.

3.2 Beam characterization

The x-ray tube was set at 150 kVp (the maximum voltage available) and tube current at 500 µA to obtain a sufficient tube output for the measurement. The added filtration was fixed to 0.2 mm Cu in order to gain a satisfying beam hardening, removing photons of very low energy that deposit energy at the surface of the irradiated medium.

The HVL in combination with the tube potential was used to characterize the spectrum: measurement of HVL were accomplished. To obtain good irradiation geometry, according to AAPM TG-61 protocol for kilovoltage x-ray dosimetry [26], the source was placed as far as possible from the ionization chamber to avoid as best as possible any scatter contributes to the detector. Chamber was put at 81 cm from the source and the beam was collimated with tungsten bar to shape the x-ray beam so that only the chamber was irradiated.

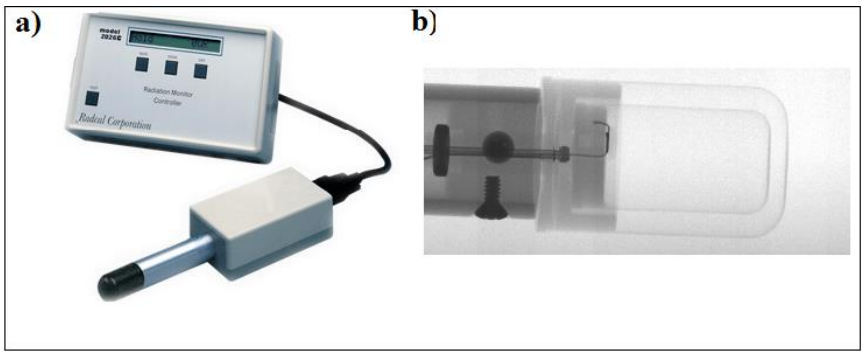

Figure 3.5 a) Ionization chamber Radcal 20X6-6 with the control unit Radcal 2026C. (http://radcal.com/ion-chambers/). b) Radiography of the chamber at 80 kVp, 250 µA.

For these measurements a fully guarded ionization chamber Radcal 20X6-6 (Radcal Corporation) in combination with a control unit Radcal 2026C was used (Figure 3.5). The chamber was used in mode "Rate" and measured the exposure rate (mR/min) with a maximum resolution of 1 mR/min (1R = 8.77 mGy in dry air).

Figure 3.6 show the experimental set-up for HVL measure: photon beam attenuation was achieved placing copper filters of variable thickness between the chamber and the source. Copper leaf were product by Goodfellow® (http://www.goodfellow.com) and had a guaranteed purity of 99.95%.

HVL was obtain measuring exposure rate with (I) and without (I_0) copper layer absorber on varying of copper thickness. Logarithm of the ratio I/I_0 was plotted as function of the copper thickness, and the HVL was obtain through linear fit, as follow:

$$\frac{1}{2} = \frac{I}{I_0} = e^{-\mu x} \rightarrow \ln 2 = \mu \cdot HVL \rightarrow HVL = \frac{ln2}{\mu}$$

Figure 3.7 exhibit linear fit achieved though Origin 8. The linear fit allowed interpolation to match the correct value of HVL (corresponding to the value of 0.693 on ordinate axis).

For a 150 kVp beam filtered with 0.4 mm Cu measured HVL was:

HVL= 0.406 ± 0.002

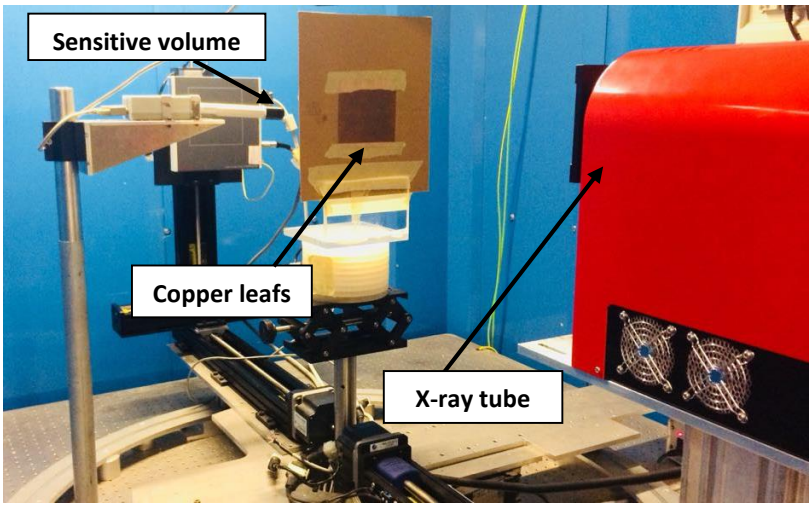

Figure 3.6 Experimental set up for HVL measurement. The chamber to x-ray tube distance was fixed at 81 cm. The copper leafs were positioned with a homemade support.

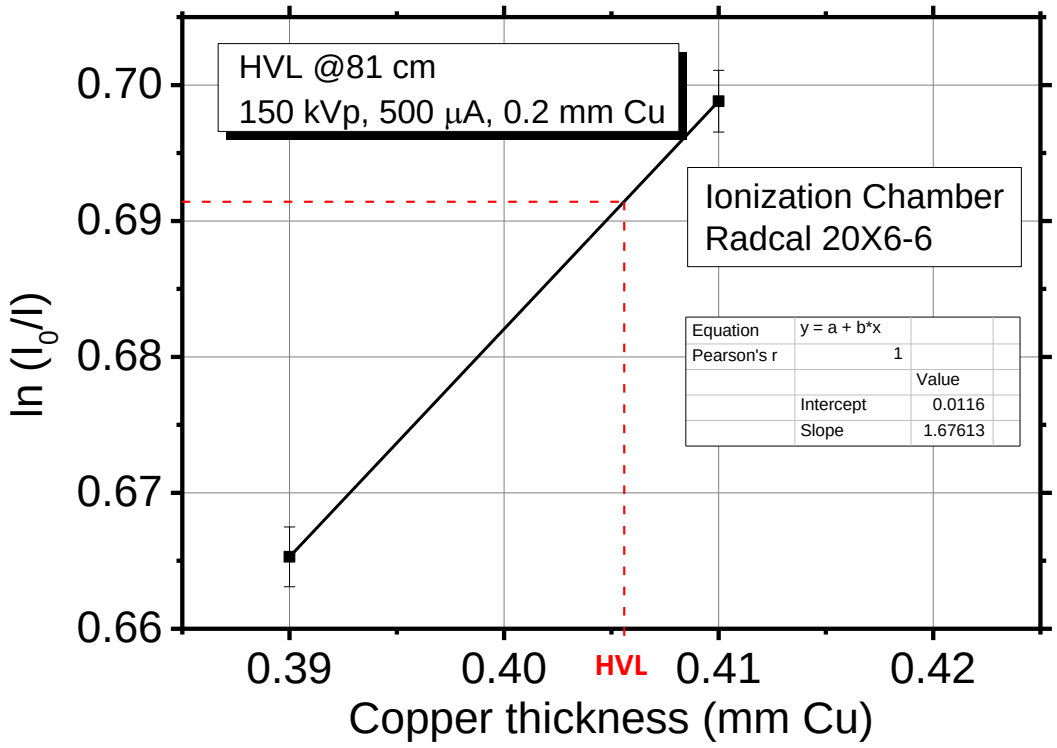

Figure 3.7 The graph shows on ordinate axis the logarithm of the ratio between two measures of exposure ratio (with and without copper layer on varying tichness) as function of copper thickness. Linear fit was used to match the correct value of HVL. Error bars on the graph describe standard deviation of the measures.

3.3 Experimental measurements at 150 kVp

The purpose of measurements was to evaluate radial dose profiles and dose distributions in a PE breast phantom (14 cm diameter, 20 cm tall) irradiated in a circular orbit of 360 degrees around cylinder central axis, with a collimated x-ray beam at 150 kVp.

Dose radial profiles depend on beam collimation, so beam height was fixed at 1.4 cm (to irradiate completely the chamber) and different beam width at were accomplished: 1.4 cm, 2.1 cm, 7.0 cm, 15 cm.

Beam collimation was evaluated at isocenter of the system because in the MC code were required as parameters beam height and width at isocenter. Tungsten leafs were placed at x-ray tube exit window to realize beam collimation.

In order to check beam size a PMMA cylindrical phantom (14 cm diameter, 20 cm height) was placed at isocenter of the system and irradiated. Source-to-isocenter distance (SID) was 37 cm. This phantom was selected since it had the same diameter of the PE cylinder used for radial

profiles measurements. The PMMA phantom was composed of two semi-cylinders to allow the placement of the radiochromic films XR-QA2 and provided a cylindrical hole along the cylinder axis for the insert of ionization chamber (unutilized for this measurements) (Figure 3.8). Irradiation induced colour change of the film, so it was possible to measure beam size at isocenter with great precision.

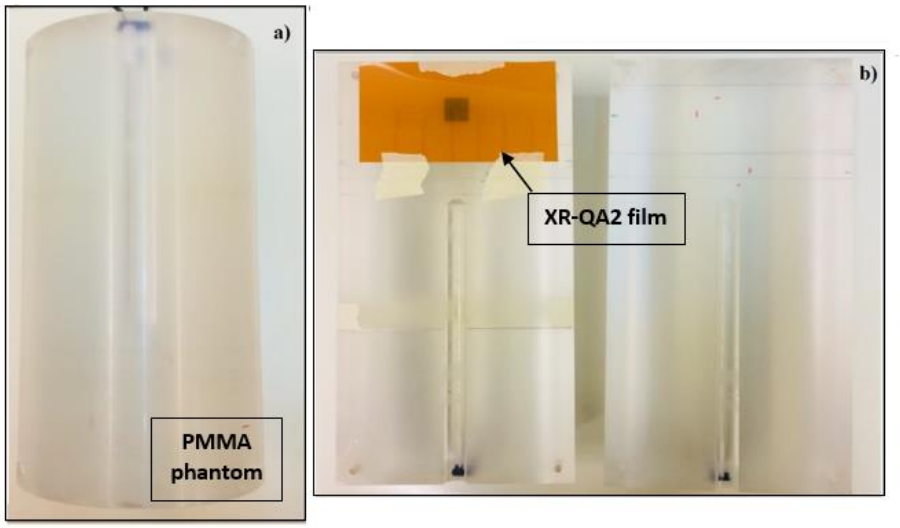

Figure 3.8 Photographs show: a) The PMMA cylindrical phantom (14 cm diameter, 15 cm tall). b) Midplane faces of cylindrical PMMA phantom with the XR-QA2 film inserted in place. The radiochromic film had change his colour in the irradiated zone, so was possible measure the beam size at isocenter..

After checking beam collimation, the PE phantom was fixed at isocenter (the axis of rotation coincided with the cylinder axis) and it was irradiated with the x-ray beam in a full circle trajectory. During the irradiation, the ionization chamber was allocated in a hollow cavity while the other holes were filled with PE bars. Measures were achieved for each radial position (Figure 3.9).

The rotation speed was 2.57 degrees/s, so the total time of irradiation was 140 s for a fully circle trajectory (for delivering 30 mGy at the central axis of the cylinder when the beam size at isocenter was 1.4×1.3 cm^2).

Dose to water D_w was measured with a UNIDOS® E Universal Dosemeter (Figure 3.10) connected to the Semiflex chamber by irradiating these at each position during a complete rotation of the x-ray tube. The radial dose profile was evaluated with the x-ray beam collimated to 1.4 cm vertically and to 1.4, 2.1, 7 or 15 cm horizontally.

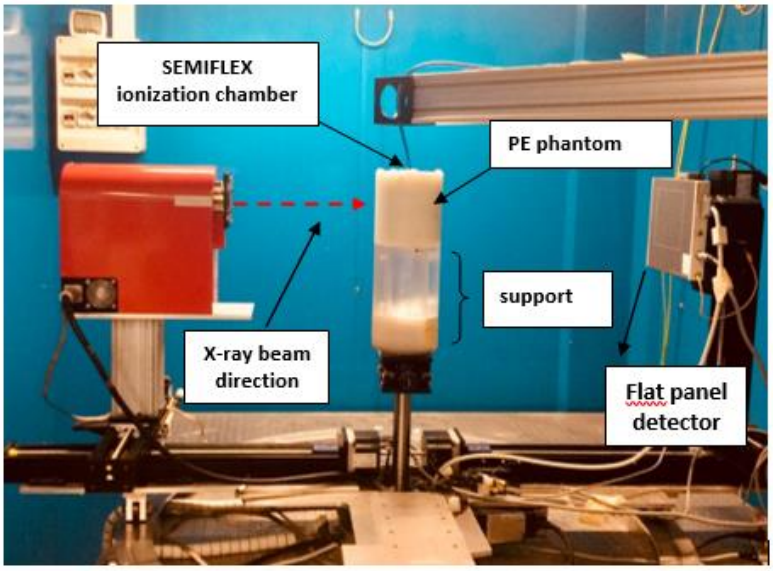

Figure 3.9 Photograph show experimental set-up for the PE phantom irradiation with the kV-EBRT technique. The cylinder was placed at isocentre of the gantry (at 37 cm from the focal spot). Ionization chamber was allocated in a cylindrical hole. Flat panel detector was unutilized during measurements, but was used in a preliminary step, to control the chamber was completely irradiated.

Measured D_w was then corrected for the FTP as follows:

$$D_w^{Corr} = D_W \cdot FTP$$

The uncertainty on D_w, following the IAEA protocol, is equal to 1.5%.

The experimental results were compared with those obtained via MC simulation, in order to have an experimental validation of the code developed to study the kV-EBRT technique.

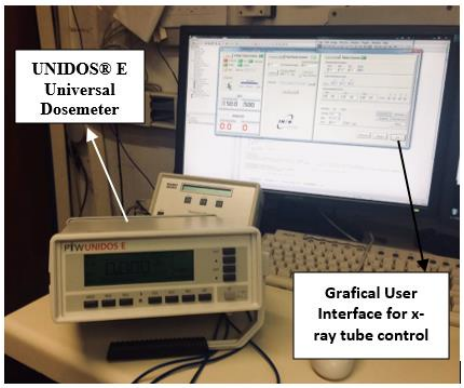

Figure 3.10 UNIDOS® E Universal Dosemeter connected with Semiflex ionization chamber. On the PC monitor the Graphical User Interface developed in house to control the bCT scanner.

3.4 MC simulations with a polychromatic beam at 150 kV

The MC code reproduced the experimental irradiation geometries in order to achieve a comparison between experimental results and MC simulations. A x-ray source at 150 kV (HVL = 0.4 mm Cu) generating a conic photons beam was simulated. The polychromatic spectrum was calculated through TASMICS tool and it was given as input to the MC code (Figure 3.11). The size of the x-ray source was varied according to the experimental cases. The rotational irradiation along 360 degrees was reproduced to obtain simulated radial dose profiles in the 14 cm diameter PE phantom. Table 3.1 summarizes the parameters set for these simulations.

Energy spectrum	150 kVp
Half value layer	0.4 mm Cu
Material	Polyethylene
Phantom dimensions	14 cm diameter, 15 cm height
Beam height	1.4 cm
Beam width	1.4 cm, 2.1 cm, 7 cm,15 cm
Number of photons	10^8 for all types of simulations
Scoring resolution	$0.1 \times 0.1 \times 0.1$ cm^3
Source-to-isocenter distance	37 cm

Table 3.1 Characteristics of simulations performed with polychromatic x-ray beam of 150 kVp irradiating a PE cylinder as the experimental irradiation geometries.

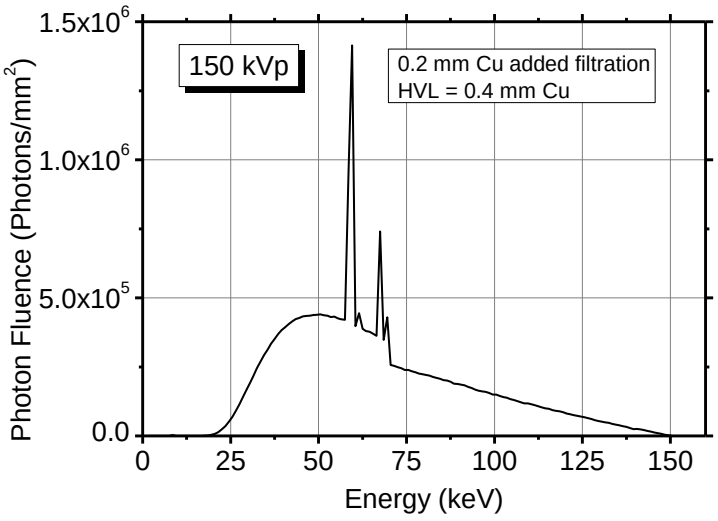

Figure 3.11 Polychromatic spectrum used for simulations: 150 kVp x-ray beam filtered with 0.2 mm Cu (half value layer 0.4 mm Cu) given by TASMICS tool. Energy resolution 1 keV. The image shows photon fluence vs energy.

3.5 MC simulations vs experimental measurements at 150 kVp

A comparison between simulated radial dose distribution and experimental measurements was shown in Figure 3.12.

The dose was expressed in terms of percentage of central dose as a function of radial distance from the central axis of the PE cylinder. For the MC simulations thr dose deposited was scored in the slices directly irradiated by the x-ray beam and radial dose profiles were derived for different beam widths.

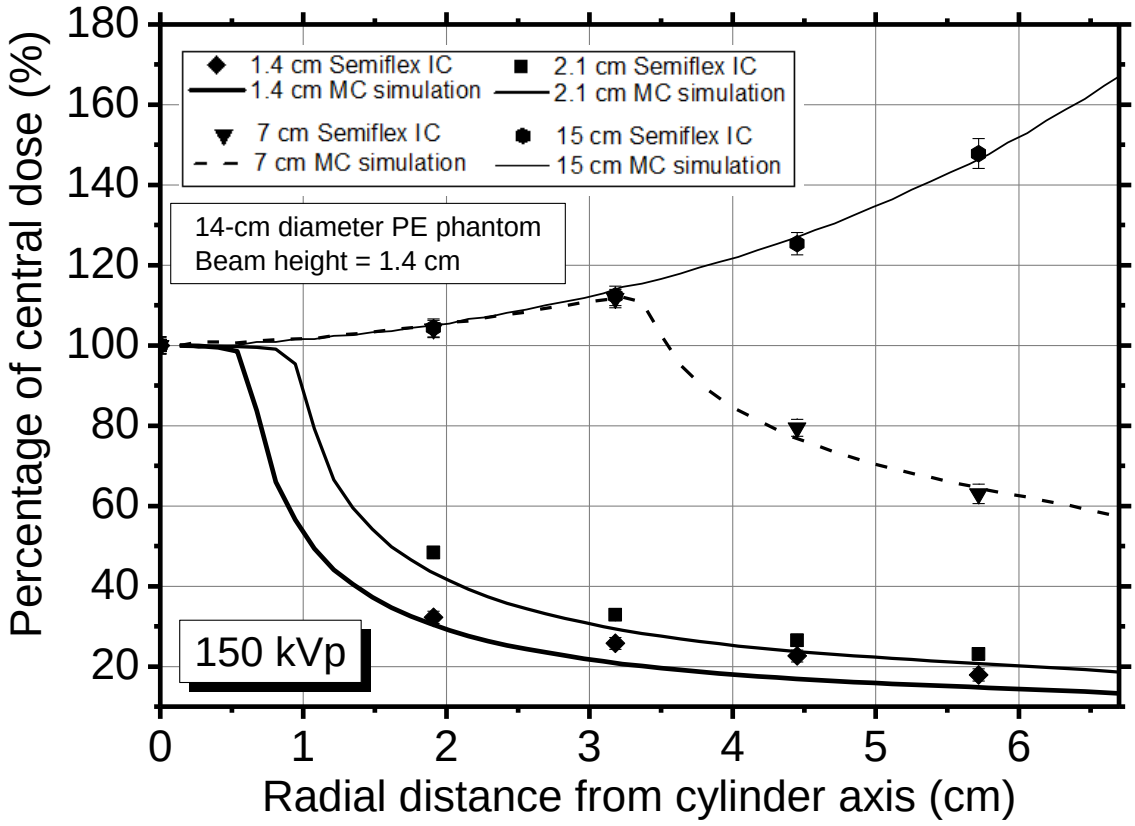

Figure 3.12 Comparison between the measured (symbols) and MC simulated (lines) radial profiles. Percentage of central dose was plotted as function the radial distance in a 14 cm diameter PE cylindrical phantom for beam width of 1.4, 2.1, 7, 15 cm. Error bars on the graph indicate standard deviation of measurements.

A center-to-periphery dose ratio of 164%, 58%, 19%, 13.5% was estimated via MC simulations for beam width collimation of 15, 7, 2.1, 1.4 cm.

The mean percentage difference (± standard deviation) in radial dose deposition between the simulations and measurements made with a Semiflex ionization chamber was reported in Table 3.2. The comparison indicates a good agreement between simulations and measurements. A

mean percentage difference of 2.2 % ± 2% and 0.9% ± 0.4% was evaluated for a collimated beam of 7 cm and 15 cm respectively.

Beam collimation width (cm)	Mean percentage of difference (%)
1.4	21.6 ± 13.5
2.1	12.6 ± 0.9
7	2.2 ± 2
15	0.9 ± 0.4

Table 3.2 Mean percentage difference between radial dose profiles simulated with the MC code and measured with the Semiflex ionization chamber.

3.5 MC simulations vs experimental measurements at 300 kVp

A further validation of the MC code was achieved by comparing the experimental measurements performed in a previous work [24] with the MC simulations developed in this thesis work.

Measurements were performed with the orthovoltage x-ray tube available at Physics Department of Naples. A Siemens Stabilipan 2 orthovoltage x-ray tube at 300 kVp spectrum with THII (1 mm Al +0.25 mm Cu +1.2 mm Sn), addition filtration of 3.12 mm Cu (HVL = 4.25 mm Cu), was used. To set the beam collimation 2 lead stripes of 1 cm of thickness were placed downstream of the Cu filtration.

Figure 3.13 shows the experimental set-up: the same PE cylindrical breast phantom used in this work was placed in the x-ray beam, a cylindrical ionization chamber (Radcal® 10.3 CT, 1.3 cm diameter and 10 cm height) inside allowed dose measure for each radial position (Figure 3.13 a).

Due to the static x-ray tube housing we rotate the phantom in order to reproduce the same geometry of rotational kV radiotherapy. So, rotation was achieved by using a step motor rotation stage in combination with PI® (Physik Instrumente) Apollo motion driver and software, to set velocity and acceleraction (Figure 3.13 b). A speed of 360 deg/360 s was selected.

Measured radial dose profiles were achieved with various collimation widths (1, 3, 7, 14 cm) while vertical collimation was 10 cm corresponding to the height of the ionization chamber.

In this thesis, De Lucia simulated the experimental geometry via MC code to compare simulations with experimental data. The starting Geant4 code was written for breast CT simulation and was based on G4EmLivermorePhysicsList, based upon Livermore data [26]. The code was adapted by De Lucia for the kV-EBRT simulation. The 300 kVp (HVL = 4.25 mm

Cu) spectrum was calculated with the SpeckCalc software (Figure 3.14) and a 14 cm voxelized (anisotropic voxels of 0.1 × 0.1 × 1 cm^3) PE phantom was implemented in the simulations.

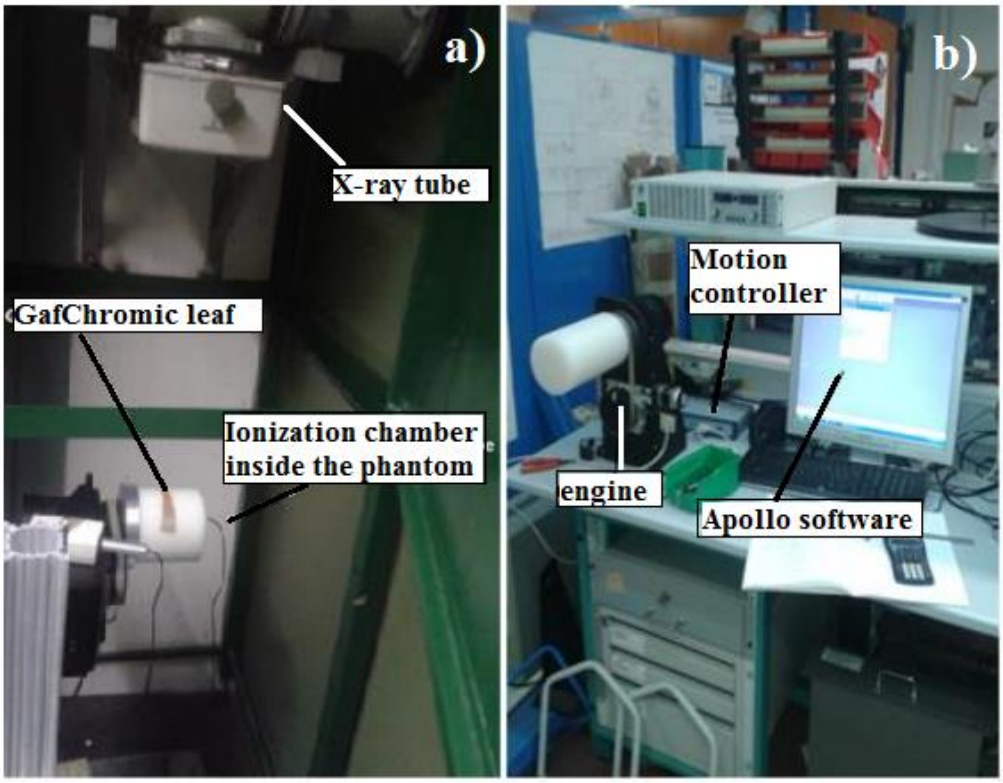

Figure 3.13 a) Photograph showing the phantom fixed to rotation stage. The distance of phantom from source was 94.5 cm and rotating knobs on collimation block allowed beam shaping to irradiate whole or partially the phantom. Inside the phantom an ionization chamber was allocated and a radiochromic film was inserted in order to set collimation width b) Rotation stage and software used to set rotation speed [26].

Figure 3.15 is shown comparison measured vs simulated dose radial profiles realised by De Lucia in his thesis.

De Lucia found for 1 cm collimation a mean percent difference (± standard deviation) of 18±8%, a better agreement was found for 3 cm (8±6%), 7 cm (3±3%) and 14 cm collimation (2±1%), respectively [26].

The same irradiation geometry of the previous study was implemented in the MC code developed in this thesis and the 300 kVp was calculated via SpekCalc software, as De Lucia's work. Figure 3.16 show a perfect superposition between the spectrum used for MC simulations in this study (red line) and the previous one used by De Lucia (black line).

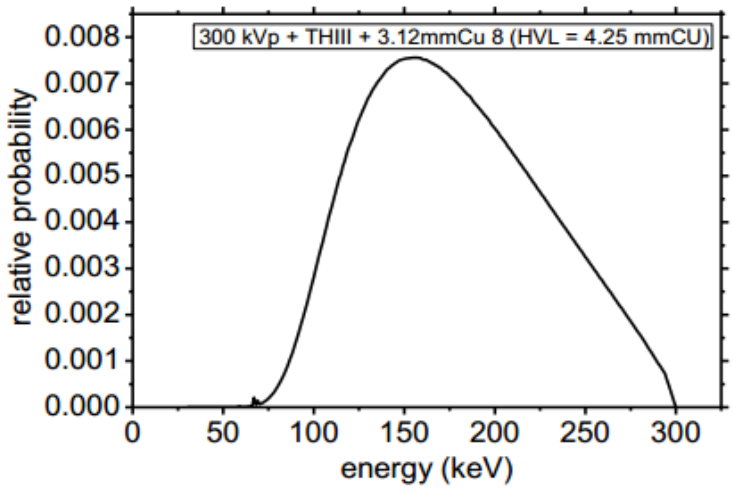

Figure 3.14 300kVp (HVL=4.25mmCu) spectrum used for measurements filtered with THIII filter 1.2 mmSn + 0.25 mm Cu + 1 mm Al) and additional 3.12 mm Cu. Image shows relative probability for x-ray photons on varying energy. Spectrum histogram was normalized.

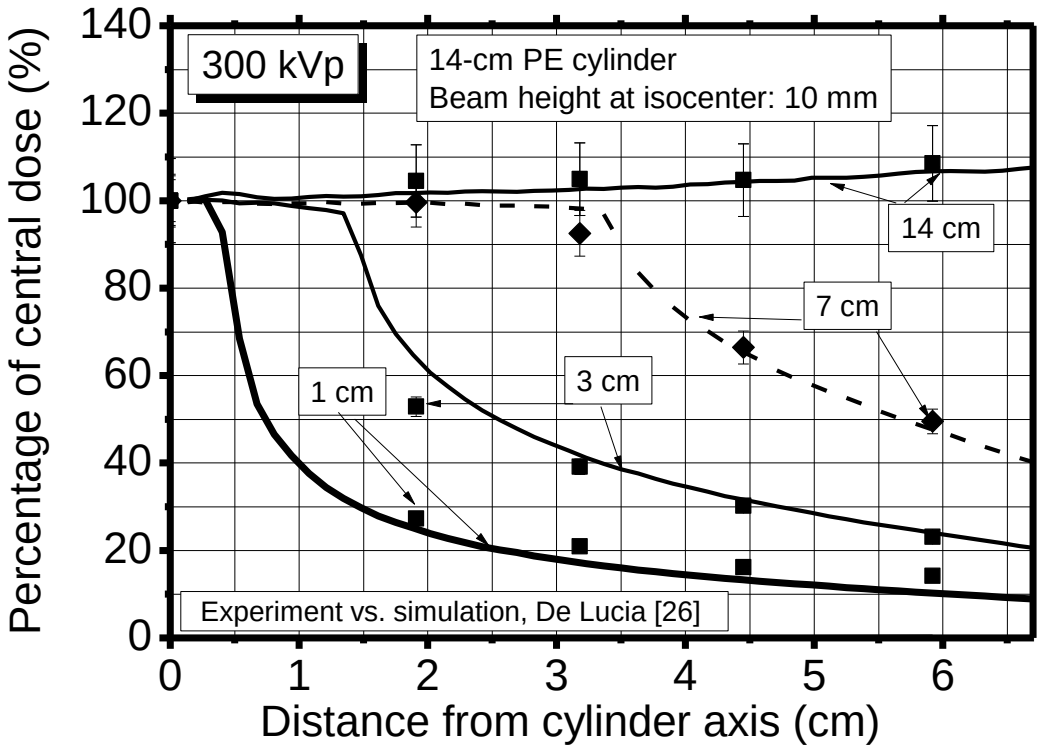

Figure 3.15 Comparison between measured and simulated dose distributions, four profiles with varies collimation widths in the horizontal direction. Cylindrical polyethylene phantom 14 cm wide and 15 cm tall was irradiated with a 10 cm beam width in vertical direction. Source was at 94.5 cm. Source used into simulations was polychromatic (300 kVp HVL=4.25 mmCu to recreate experimental geometry [26].

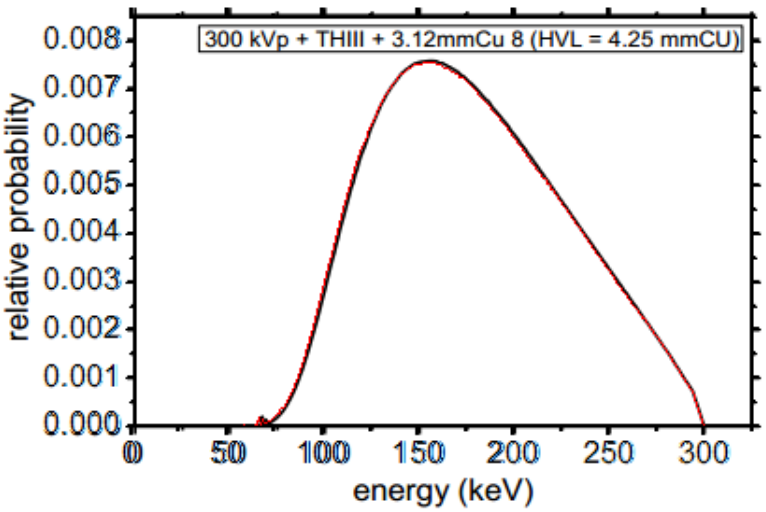

Figure 3.16 Superposition of SpeckCalc spectrum used for MC simulation in this work (red line) and in De Lucia' work (black line).

Energy spectrum	300 kVp
Half value layer	4.25 mm Cu
Material	Polyethylene
Phantom dimensions	14 cm diameter, 15 cm height
Beam height	10 cm
Beam width	1 cm, 3 cm, 7 cm,14 cm
Number of photons	10^8 for all types of simulations
Scoring resolution	$0.1 \times 0.1 \times 1$ cm^3
Source-to-isocenter distance	94.5 cm

Table 3.3 Characteristics of simulations performed with polychromatic x-ray beam of 300 kVp irradiating a PE cylinder as the experimental irradiation geometries of [26].

Table 3.3 summarizes the parameters of the simulation with the polychromatic spectra at 300 kVp. In these simulations the phantom was modelled as a "continuous" object and the dose deposition and event position information were scored in a 3D matrix overlapping with the cylinder, in opposition to the voxelized phantom of the previous study.

Figure 3.17 shows a comparison between measured radial profiles and the simulated ones. The mean percentage difference (± standard deviation) between measurements and simulations were 1.8 % ± 0.5% for 14 cm beam width, 2.7% ± 3.0% for 7 cm beam width, 9.7 ± 6.2 % for 3 cm beam width, and 20% ± 7% for 1 cm beam width. A good agreement was found with the

previous experimental study and MC simulations. A maximum deviation of 2% was observed from the previous comparison.

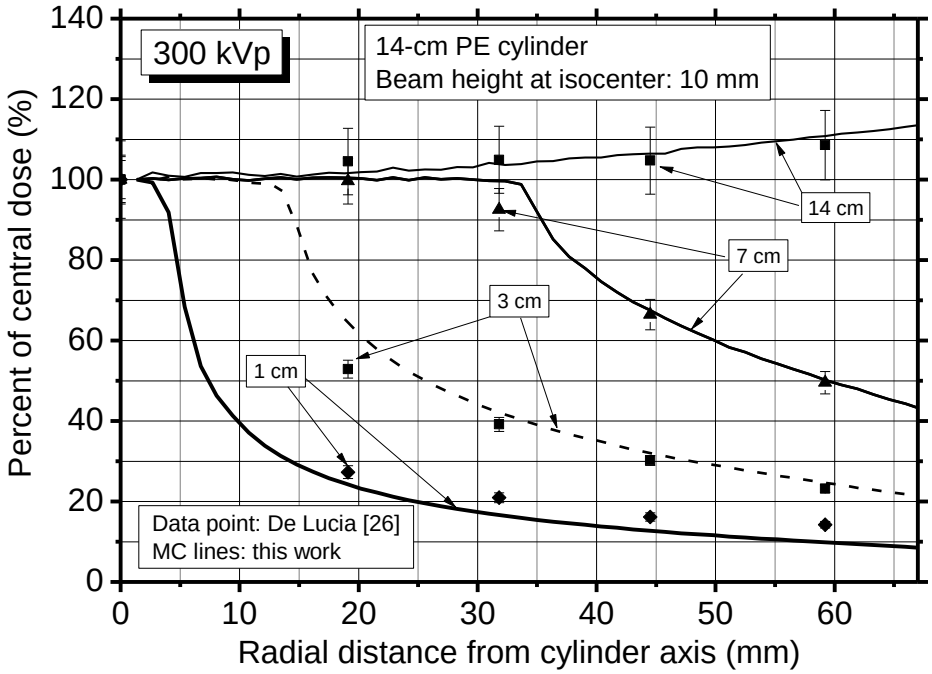

Figure 3.17 Measured vs simulated dose distributions, for four profiles with varies collimation widths in the horizontal direction. Cylindrical polyethylene phantom 14 cm wide and 15 cm tall was irradiated with a 10 cm beam width in vertical direction. Source was at 94.5 cm. Source used into simulations was polychromatic (300 kVp HVL=4.25 mmCu to recreate experimental geometry.

3.6 Clinical implementation of the kV-EBRT technique

The study of the kV-EBRT was taken into consideration by the Medical Physics group due to the availability of a prototype since the existence of a prototype of bCT scanner in Medical Physics laboratory.

The research about kilovoltage RT and the possible development of this new technique for irradiating small mass in breast cancer treatment will be continued.

A possible implementation of kV-EBRT in this prototype may include an orthovoltage x-ray tube (e.g. Xsthral 200) on the rotating gantry.

Xsthral 200 is an the x-ray therapy system designed to be purchase. It is commonly used for treating many superficial skin cancers and dermatological conditions such as psoriasis. In addition, the Xstrahl 200 enables orthovoltage therapy for palliative care, including treatment of soft tissue metastases and secondary lesions (Figure 3.18).

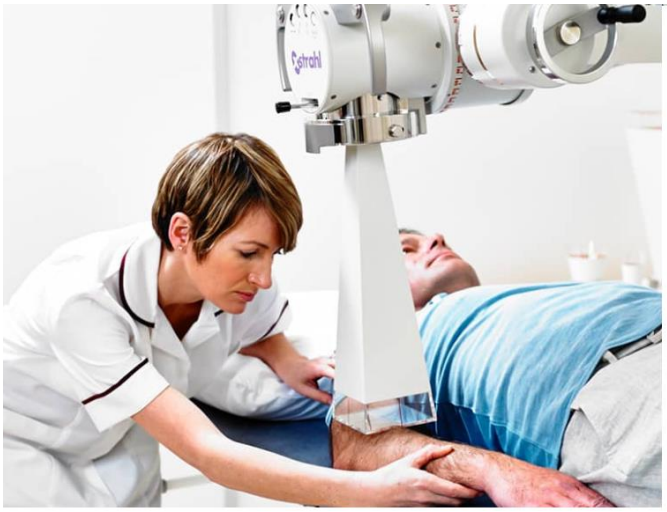

Figure 3.18 The photograph show a patient on a bed. The Xsthral 200 is used when reviewing skin lesions and getting orthovolatge therapy procedure ready [27].

It uses tubes with 20 - 200 kV voltage levels and 0 - 30 mA currents that can work at up to 3 kW in power at their most intense.

Conclusions

This work of thesis was born to investigate the possible developments of the kV-EBRT technique. A dedicated MC code was realized and validated with reference to literature data reported by Prionas et al. in pioneering paper introducing this technique.

Simulations with an orthovoltage x-ray beam rotating around the axis of the phantom demonstrated that that the shape of the dose distribution in a PE cylinder phantom depends on beam collimation. A narrow beam in the horizontal plane produces a dose distribution peaked in the center of rotation. On the contrary, a broad beam irradiating the whole phantom produced a cupping dose profile, with high dose at surface of the phantom, so producing no "skin sparing".

In particular, we demonstrated that it is possible to have a pheryphery-to-centre dose ratio of about 10% of the central dose value (in contrast to the about 140% for a 14 cm beam width at isocentre) evaluated at 320 kVp, for a beam collimation at the centre of rotation of 1.5 cm × 2 cm.

The dose distribution in a tumor phantom was simulated for breast of different glandular composition. Partial breast irradiation was studied for three cases of interest: a deep lesion, a middle-placed lesion and a superficial lesion.

A specific investigative goal was to assess the lesion-to-skin ratio for an irradiation around the axis of the lesion. For a deep lesion the edge dose ranged between 10.6-11.3 % of the maximum dose deposit. A sufficient skin sparing was achieved for the irradiation of a tumor placed at 3.75 cm from the breast surface, where a lesion-to-skin-ratio of about 16% was observed. For a lesion near the surface the lesion-to-skin ratio was about 34% of the maximal dose deposit.

To reduce the dose to the skin a bolus of equivalent tissue was implemented in the simulation geometry, at direct contact with the breast phantom. This structure reduced by 5% the dose to the skin in superficial lesions treatment with the kV-EBRT technique. Future study are needed to optimize the bolus in order to reduce to an acceptable level the dose occurring at the skin.

An experimental validation of the MC code was accomplished in the Medical Physics laboratory of University of Naples "Federico II" and comparison with a previous work was obtained.

This study, through a validated MC code, provided an independent proof of concept of the kV-EBRT technique applied to breast cancer, as proposed in 2012 by J. Boone. This study extended

the previous literature report by performing investigation on tumor treatment at different depths and for different breast compositions.

References

[1] www.wcrf.org

[2] www.radioterapiaitalia.it

[3] MatjažJeraj, Vlado Robar *Multileaf collimator in radiotherapy*. Radiol Oncol (2004); 38(3): 235-40.

[4] R. K. Funk, A.L. Stochkam, N.N. Issa Laac. *Basics of Radiation Therapy*. In: Clinical Cardio-oncology, J.Herrmann (Ed.), Elsevier, 2016.

[5] C.W. Taylor et al. *Cardiac dose estimates from Danish and Swedish breast cancer radiotherapy during 1977-2001*. Radiother Oncol. (2011); 100(2): 176-183.

[6] Taylor C.W. et al. *Cardiac dose from tangential breast cancer radiotherapy in the year 2006.* Int JRadiat Oncol Biol Phys. (2008); 72: 501-507.

[7] Pogdorsak E.B., *Radiation oncology physics: a handbook for teachers and students*. (2005); ISBN 92-0-107304-6.

[8] Palmer A.L., Pearson M., Whittard P., McHugh K.E., Eaton D.J., Current status of kilovoltage (kV) radiotherapy in the UK: installed equipment, clinical workload, physics quality control and radiation dosimetry. Br J Radiol. (2016); 89:20160641.

[9] R.Hell, L. Holloway et al. *Advances in kilovoltage x-ray beam dosimetry*. Phys.Med.Biol. (2014); 59(6): R185-R231.

[10] Prionas N.D., McKenney S.E., Stern R.L. and Boone J.M. *Kilovoltage rotational external beam radiotherapy on a breast computed tomography platform: a feasibility study*. Int. J. Rad. Oncol. Biol. Phys. (2012) 84(2), 533–539.

[11] J.M. Boone, T.R. Nelson, K.K. Lindfors, J.A. Seibert *Dedicated breast CT: radiation dose and image quality evaluation.* Radiology (2001); 221(3): 657-667.

[12] A. Sarno, G.Mettivier, P.Russo, *Dedicated breast computed tomography: Basics aspects*, Med. Phys. (2015); 42(6): 2786-2804.

[13] P. Deseyne et al. *Whole breast and regional nodal irradiation in prone versus supine position in left sited breast cancer.* Radiation Oncology (2017); 12:89.

[14] Bazalova-Carter M., Weil M.D., Breitkreutz D.Y., Wilfley B.P., Graves E.E. *Feasibility of external beam radiation therapy to deep-seated targets with kilovoltage x-rays*, Med. Phys. (2017); 44(2): 597-607.

[15] Breitkreutz D.Y., Weil M.D., Zavgorodni S., Bazalova-Carter M. *Monte Carlo simulations of a kilovoltage external beam radiotherapy system on phantoms and breast patients.* Med Phys. (2017); 44(12): 6548-6559.

[16] F. Di Lillo, G. Mettivier, R. Castriconi, A Sarno, A. W. Stevenson, C. J. Hall, D.Hausermann and P Russo. *Synchrotron radiation external beam rotational radiotherapy of breast cancer: proof of principle.* J. Synchrotron Rad. (2018); 25: 857–868.

[17] S. Agostinelli et al. *Geant4—a simulation toolkit,* Nuclear Instruments and Methods in Physics Research (2003); A 506: 250–303.

[18] https://www.nist.gov/pml/xcom-photon-cross-sections-database

[19] E. S. Poon *Validation of the GEANT4 Monte Carlo code for radiotherapy applications,* (2004), thesis of Degree Master in Science, McGill University, Canada.

[20] http://spekcalc.weebly.com/

[21] https://imagej.nih.gov/ij/download.html.

[22] https://www.origin.com/ita/en-us/store/download.

[23] https://products.office.com/en/excel.

[24] P. De Lucia. *Kilovoltage rotational external beam radiation therapy (kV-EBRT) for breast cancer treatment*. Master Thesis in Medical Physics at University of Naples Federico II, 2015, www.infn.it/thesis.

[25] http://www.ptw.de/semiflex_chambers.

[26] C.M. Ma. et al. *AAPM protocol for 40–300 kV x-ray beam dosimetry in radiotherapy and radiobiology.* Med. Phys. (2001); 28(6): 868-893.

[27] https://xstrahl.com/

Ringraziamenti

Giunta alla fine di questo lungo percorso, guardandomi indietro, mi rendo conto che questo traguardo non sarebbe stato possibile senza una lunga lista di persone che mi hanno accompagnata “prendendomi per mano”.

In primis c’è il Prof. Russo, una presenza fondamentale nel laboratorio di Fisica Medica, un mentore, la guida del mio percorso.

Ringrazio il Prof. Giovanni Mettivier per i suggerimenti e humor.

Antonio e Francesca, senza di voi non so come avrei fatto, sempre disponibili a dispensare consigli e quant’altro. Voglio ringraziare il mio correlatore Prof. Roca, per le domande che stimolavano il mio impegno.

Non posso non citare le “Tesiste”, voi sapete perché. Grazie, questi mesi sono stati folli, ma belli.

APPENDIX A- Terms describing methods of radiation therapy